DESIGN AND ANALYSIS OF SUB-THZ METAMATERIAL STRUCTURES FOR ABSORBER, SENSOR, AND SWITCH APPLICATIONS

A THESIS SUBMITTED TO THE BOARD OF GRADUATE PROGRAMS

OF

MIDDLE EAST TECHNICAL UNIVERSITY, NORTHERN CYPRUS CAMPUS

BY

AHMET FARUK

IN PARTIAL FULFILLMENT OF THE REQUIREMENTS

FOR

THE DEGREE OF MASTER OF SCIENCE

IN

SUSTAINABLE ENVIRONMENT AND ENERGY SYSTEMS

JUNE 2019

Approval of the Board of Graduate Programs _____

Prof. Dr. Gürkan Karakaş
Chair person

I certify that this thesis satisfies all the requirements as a thesis for the degree of Master of
Science

_____

Assoc. Prof. Dr. Ceren İnce
Program Coordinator

This is to certify that we have read this thesis and that in our opinion it is fully adequate, in scope and quality, as a thesis for the degree of Master of Science.

_____

Assoc. Prof. Dr. Cumali Sabah
Supervisor

Examining Committee Members

Assoc. Prof. Dr. Cumali Sabah	Electrical and Electronics Engineering Dept. METU NCC _____
Assoc. Prof. Dr. Soydan Redif	Electrical and Electronics Engineering Dept. EUL _____
Assoc. Prof. Dr. Volkan Esat	Mechanical Engineering Dept. METU NCC _____

I hereby declare that all information in this document has been obtained and presented in accordance with academic rules and ethical conduct. I also declare that, as required by these rules and conduct, I have fully cited and referenced all material and results that are not original to this work.

Name, Last name: Ahmet Faruk

Signature :

ABSTRACT

DESIGN AND ANALYSIS OF TWO UNIQUE SUB-THZ METAMATERIAL STRUCTURES FOR ABSORBER, SENSOR AND SWITCH APPLICATIONS

Faruk, Ahmet

M.Sc. Sustainable Environment and Energy Systems Program

Supervisor: Assoc. Prof. Dr. Cumali Sabah

June 2019

Innovations in the manufacturing technology has led to an increase for the utilization of Terahertz (THz) region, which is also the most recent explored region of the electromagnetic spectrum. Although THz region is being used widely in various applications such as sensing, detecting, biological, and chemical, the region still requires further research and development of advanced devices. Metamaterials (MTMs) that are unnatural artificial materials are optimal for enhancing such devices operating by THz waves. In this context, Sub-THz MTM fishnet and absorber structures are designed and analyzed for the application of the THz region. Subsequently, the designs are theoretically analyzed and numerically evaluated with the verification of the perfect absorption rates. Additionally, the designs are tested as a MTM sensor that uses the resonant shifts to find the unknown materials. Moreover, two meta-switches are presented by doping of a photoconductive silicon to the proposed designs. Ultimately, two unique MTM structures have been introduced to the literature to be used in the future THz MTM applications and researches.

Keywords: Metamaterial, Sub-THz, Absorber, Sensor, Tunability, Metaswitch.

ÖZ

SOĞURUCU, SENSOR VE ANAHTAR UYGULAMALARI İÇİN SUB-TERAHERTZ METAMALZEME YAPILARININ TASARIMI VE ANALİZİ

Faruk, Ahmet

Yüksek Lisans, Sürdürülebilir Çevre ve Enerji Sistemleri Programı

Tez Yöneticisi: Doç. Dr. Cumali Sabah

Haziran 2019

Üretim tekniklerindeki yenilikler elektromagnetik tayfının son keşfedilen kısmı olan Terahertz (THz) bölgesinin kullanımında artışa sebep olmuştur. THz bölgesi saptama, algılama, kimyasal ve biyolojik gibi çeşitli uygulama alanlarında kullanılıyor olmasına rağmen, bahsedilen bölge gelişmiş cihazlar için halen araştırma ve geliştirmeye ihtiyaç duymaktadır. Doğal olmayan yapay metamalzemeler (MTMs) bu gibi THz bölgesinde çalışan cihazların geliştirilmesine uygundurlar. Bu bağlamda, THz bölgesi uygulaması için alt-THz MTM balık ağı yapısı ve soğurucu tasarlanmış ve analiz edilmiştir. Sonrasında, mükemmel soğurucu kriter oranları sağlanarak, tasrımlar teorik ve nümerik olarak analiz edilmiştir. Ek olarak, tasarımlar MTM sensör olarak bilinmeyen materyallerin bulunmasında rezonans değişimlerindeki farklılıklar kullanılarak test edilmişlerdir. Ayrıca, önerilen tasarımlara foto-iletken silikon entegre edilerek, iki tane meta-anahtar sunulmuştur. Sonuç olarak, iki adet özgün MTM yapısı gelecekteki THz MTM uygulamaları ve araştırmalarında kullanılmak üzere literatüre sunulmuştur.

Anahtar Kelimeler: Metamalzeme, THz-Altı, Soğurucu, Sensor, Anahtar.

DEDICATION

I dedicate this work to my mother.

ACKNOWLEDGEMENTS

Foremost, I would like thank to my thesis supervisor, Assoc. Prof. Dr. Cumali Sabah whose immense knowledge, understanding, and patience, considerably contributed to my graduate experience. His guidance always helped me during my research and for completing of this study.

Besides my supervisor, I also would like to thank to thesis jury members: Assoc. Prof. Dr. Volkan Esat and Assoc. Prof. Dr. Soydan Redif for their valuable suggestions and constructive criticisms during this study.

I must acknowledge my senior in the metamaterial research group and workmate from Physics laboratory, Batuhan Mulla for his constructive ideas and continuous support during this study. I would also like to thank my dearest friends Ahmad Rasheed, Berkay Koyuncu, Koray Gürkaya, Muhammed Abbujubeh and Mustafa Safa Kırlı for good times and memories during this path.

I would like to express my special thanks to special person Melis Erhun.

Last but not least, I would like to thank my family for their support, and encouragement during my research.

TABLE OF CONTENTS

TABLE OF FIGURES

LIST OF SYMBOLS

THz	Terahetz
SBD	Schottyky Barier Diode
MTMs	Metamaterials
E	Electric Field ($V.m^{-1}$)
B	Magnetic Flux Density (T)
D	Electric Flux Density (C/m^2)
J	Electric Current Density (A/m)
ρ	Volume charge density (C/m^3)
ε	Electric permittivity
μ	Magnetic permeability
ω	Angular frequency
k	Electromagnetic wave vector
c	Speed of light
n	Refractive index
ρ	Reflected amplitude
τ	Transmitted amplitude

FIT	Finite Integration Method
FEM	Finite Element Method
FDTD	Finite Difference Time Domain
Z	Impedance
A(w)	Frequency dependent Absorbance
R(w)	Frequency dependent Reflectance
T(w)	Frequency dependent Transmittance
σ	Conductivity

CHAPTER 1: INTRODUCTION

The enhancement of devices that are working with electromagnetic waves are really important as we are living in a smarter world. The boundaries of the electromagnetic spectrum have been discovered and so many regions are being used for different applications, however one region is considered as the last untouched region of the whole spectrum. The devices that operate with microwave or smaller frequencies are called electronic materials, and the devices that work with visible light or higher frequencies are called photonic materials, between the photonics and electronics there is a region that is actually hard to find natural materials that interact with it. This region is called Terahertz (THz) region and the corresponding wavelength lie between 3 mm to 30 μm. As well as it is hard to produce THz waves, it is also a big challenge to develop devices that operates with THz waves. In the 21. Century the THz technology have been attracted to much interest, the technology of producing THz waves progressed lot and the attention on this region became more tense.

1.1 Terahertz Spectrum

Most of the important physical, chemical and biological processes energetically equivalent to the THz part of the electromagnetic spectrum. In Figure 1.1 the frequency and wavelength regions of electromagnetic spectrum can be seen. THz region has 0.1 to 10 THz frequency range and the corresponding wavelengths lie between 3 mm to 30 μm. As it can be seen from the figure the region lies between electronics and photonics.

However, till the beginning of 21. Century the capabilities of electronic and photonic devices were insufficient for using THz waves. So they called this region as THz gap.

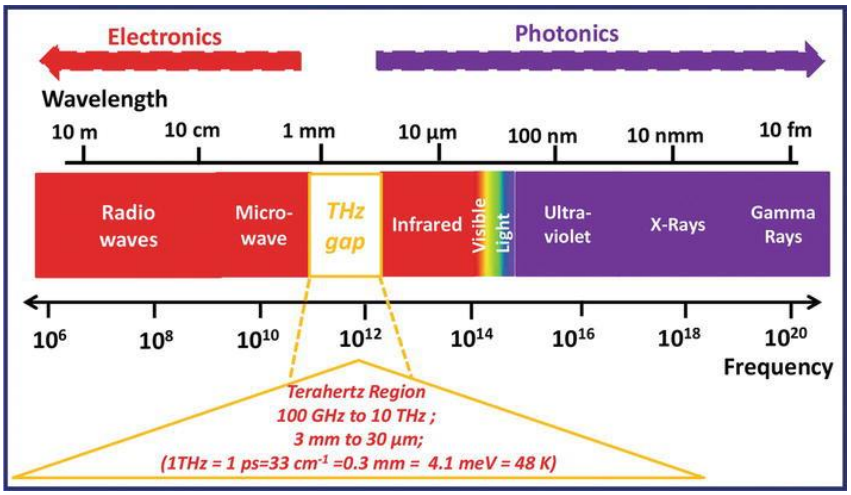

Figure 1-1 Frequency and wavelength regions of the electromagnetic spectrum [1]

With the developed manufacturing techniques in nanoscale, THz spectrum has started to be very attractive [2] [3]. In photonics the invention of quantum cascade laser which provides powerful THz waves and in electronics discovery of solid state electronic devices and Schottyky barrier diodes (SBDs), have increased the usage of THz region. At the beginning the applications were only limited with the astronomy and analytical sciences however in recent times information and communication technology (ICT), biology medical sciences, nondestructive evaluation, homeland security, quality control of foods and ultrafast computing are some the areas that uses this region [4]. There are three main reasons that make this region attractive first one is, many non-metallic and non-polar materials are transparent to THz, second reason, some compounds especially explosives

have characteristic THz spectra and the last reason is THz waves have no health risk for scanning of people. The biggest problem with Terahertz (1THz = 1012 Hz) frequency region is that most of the materials do not respond to THz radiation, and as a result it is difficult to produce tools such as switches, lenses and modulators for devices operating within that region of electromagnetic spectrum [5, 6, 7]. Another problem is the extreme atmospheric absorption due to water vapor and oxygen, the attenuation is so high that the transmission of high power THz wave is really limited [8]. In order to solve that problems, the devices should be very sensitive to THz wave and they should have advanced features which gives ability to work with the highest performance. Metamaterials are one of the best candidate for meeting the desired properties. In the next part the exotic properties of metamaterials will be described.

1.2 Metamaterials

It is hard to find materials that give responses to THz waves, in that case Metamaterials (MTMs) which are artificial materials that cannot exist naturally in nature, may help us to work with THz region. Theoretically, the properties of MTMs that has both negative permittivity and permeability (left handed materials) defined and analyzed by Veselago in 1967, he concluded that left handed materials have negative refractive index and they display reversed Doppler Effect and reversed Vavilov-Cerenkov Effect [9]. Metamaterials consist of a metallic pattern on a dielectric substrate and the electromagnetic properties of MTM can be changed by changing the geometry and selected material of both metallic pattern and dielectric substrate. At the beginning of 21. Century effects of geometry and materials on MTM properties have been studied experimentally and theoretically by

scientists. [10, 11, 12, 13]. In order to understand the response of MTMs to incoming electromagnetic waves we can assist from Maxwell Equations.

1.2.1 Maxwell Equations

The response of the material to incoming electromagnetic wave can be described with the optical properties of the material. In order to understand the interaction of electromagnetic waves and materials we have to consider Maxwell equations;

$$\nabla \times \mathbf{E} = -\frac{\partial \mathbf{B}}{\partial \mathrm{t}} \tag{1.1}$$

$$\nabla \times \boldsymbol{H} = \boldsymbol{J} + \frac{\partial \boldsymbol{D}}{\partial t} \tag{1.2}$$

$$\nabla . \boldsymbol{D} = \boldsymbol{\rho} \tag{1.3}$$

$$\nabla . \boldsymbol{E} = 0 \tag{1.4}$$

In the equations, E and H show Electric and Magnetic field respectively, and in Equations 1.2 and 1.3 D represents electric flux density. For the homogenous isotropic medium, the equations can be transformed, and D and B can be given by equations 1.5 and 1.6.

$$\vec{\boldsymbol{D}} = \boldsymbol{\varepsilon}\vec{\boldsymbol{E}} \tag{1.5}$$

$$\vec{\boldsymbol{B}} = \mu\vec{\boldsymbol{H}} \tag{1.6}$$

If the equation 1.5 and 1.6 are integrated to Maxwell equations, equations can be rewritten as shown in equation 1.7-1.10.

$$\nabla . \boldsymbol{\varepsilon}\vec{\boldsymbol{E}} = \mathbf{0} \tag{1.7}$$

$$\nabla . \boldsymbol{\varepsilon}\vec{\boldsymbol{H}} = \mathbf{0} \tag{1.8}$$

$$\nabla \times \vec{\boldsymbol{E}} = -\mu \frac{\partial \vec{\boldsymbol{H}}}{\partial \mathrm{t}} \tag{1.9}$$

$$\nabla \times \vec{\boldsymbol{H}} = \boldsymbol{\varepsilon} \frac{\partial \vec{\boldsymbol{E}}}{\partial \mathrm{t}} \tag{1.10}$$

Let's assume that electromagnetic wave propagates in the z-direction and the direction is shown by k. with the addition of frequency dependency of the magnetic field and electric field intensity the final forms of Maxwell equations are gathered.

$$\vec{E}(w, \vec{E}) = \overrightarrow{E_0} e^{-i(kz-\omega t)} \tag{1.11}$$

$$\vec{B}(\mathrm{w}, \vec{B}) = \overrightarrow{B_0} e^{i(kz-\omega t)} \tag{1.12}$$

$$\vec{k} \times \vec{E} = -\frac{w}{c} \mu \vec{H} \tag{1.13}$$

$$\vec{k} \times \vec{H} = \frac{w}{c} \varepsilon \vec{E} \tag{1.14}$$

Where $\vec{k}$ represents the electromagnetic wave vector, *w* is the angular velocity of the wave and *c* is the speed of light in free space.

1.2.2 Refractive Index

In media, the behavior of electromagnetic radiation is derived by an optical property of the material which is the combination of relative permittivity and permeability. This property is called refractive index.

$$n = \pm\sqrt{\varepsilon_r \mu_r} \tag{1.15}$$

The refractive index is usually used in Snell's Law (Equation (1.21)), and it helps to find the angle of refraction between two media when electromagnetic radiation passes between two media. The other usage of the refractive index is in the calculation of reflected (ρ) and transmitted (τ) amplitude, which is described by Fresnel's equation. Refractive index can also be explained by the ratio between the speed of light in free space and its speed within the medium.

$$n = \frac{c_0}{v} \tag{1.16}$$

$$\rho = \frac{n_1 - n_2}{n_1 + n_2} \tag{1.17}$$

$$\tau = \frac{2n_1}{n_1 + n_2} \tag{1.18}$$

Where n_1 and n_2 refer the refractive indices of the first and the second medium respectively. The Equations 1.17 and 1.18 are only valid for non-magnetic materials which

μ_r is equal to 1. However, for the magnetic materials we should integrate Impedance (Z) to the equations, where we can refer them with;

$$\rho = \frac{Z_1 - Z_2}{Z_1 + Z_2} \quad (1.19)$$

$$\tau = \frac{2Z_1}{Z_1 + Z_2} \quad (1.20)$$

The equations are well describing the interaction between the electromagnetic wave and the medium in macroscopic scale. In the microscopic especially with the dimensions lower than the wavelength of the incoming wave the hypothesis will be a bit different and metamaterials behavior can be described better.

1.2.3 Negative Refraction

When the electromagnetic radiation passes from one medium to another one, the refraction characteristic is well described by Snell's law. The refraction depends on the refractive indices of the mediums and incidence angle of the wave.

$$n_1 sin\theta_i = n_2 sin\theta_r \quad (1.21)$$

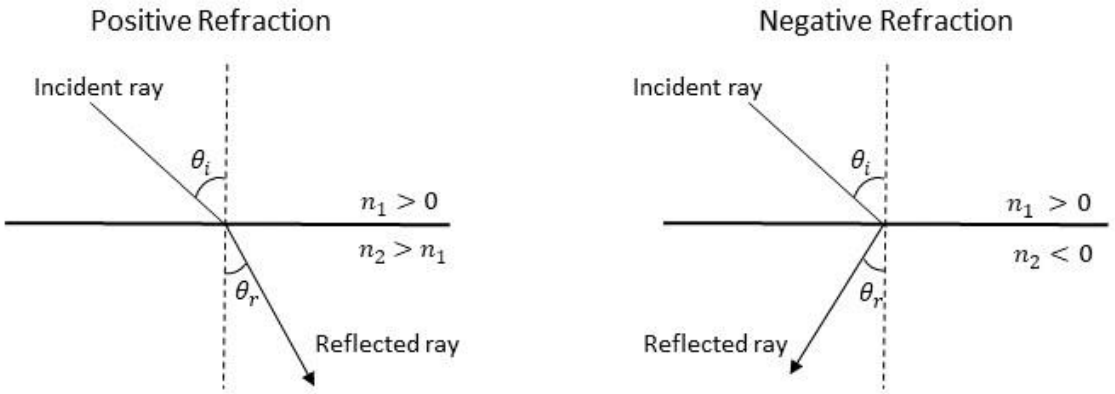

Figure 1-2 Reflection of light from a) positive medium b) from negative medium

From the Figure 1.2 it can be seen that for negative refractive index (NRI) material the refraction of the incident light is directly opposite side of the positive index materials.

Negative refraction can be achieved by negative permittivity (ε) and negative permeability (μ). Complex forms of permittivity and permeability derives the characteristic of the material. Below, the equations for complex μ and ε are given.

$$\varepsilon(w) = \varepsilon'(w) + i\varepsilon''(w) \quad 1.22$$

$$\mu(w) = \mu'(w) + i\mu''(w) \quad 1.23$$

As it can be seen from the equations complex permittivity and complex permeability are frequency dependent which means that their values are changing with the frequency of incoming radiation. Most naturally existing materials have both permittivity and permeability positive at the same time and that materials are called Double Positive Medium **DPS,** for example all dielectrics. If the real part of the permittivity is negative

and the real part of permeability is positive, these materials are called Epsilon Negative Medium **ENG** materials. Opposite to this, when the permeability is negative and the permittivity is positive, they are termed as Mu Negative Medium **MNG**. Besides, materials with both negative permittivity and permeability do not naturally exist and they are named as Double Negative Medium **DNG** or left handed materials. In the Figure 1.3 the classification of Materials according to their optical properties are given.

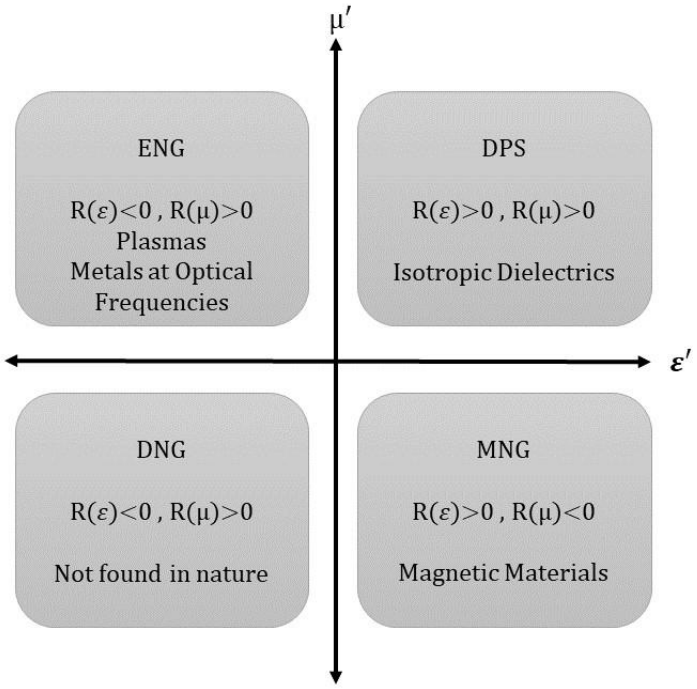

Figure 1-3 Classification of Materials according to their permittivity and permeability

1.3 Literature Review

Nowadays, with the help of previous studies on theoretical and experimental validation of metamaterials, MTMs are being used in many fields like communication, energy, biology etc. [14]. Also, They have been used in many different applications like lenses, sensors, filters and antennas [15, 16, 17]. Besides those applications, imaging technology is

another area for MTMs, especially single pixel imaging, with using active tunable filters [18, 19]. Within the context of this thesis, a literature review is done by focusing on the absorber, sensor, tunability and switch applications. The literature review is essential for better understanding the concept, and contributing to the missing parts in the literature.

From literature, it can be seen that the focus is more on, increasing absorbance of the metamaterial structures [20]. After the invention of characteristics of metamaterial absorbers by Landy [21], the attention is moved toward increasing the absorption rates. The applications also jumped to THz region; He presented a metamaterial absorber which gives two absorption peaks at terahertz frequency range. They have 82.8% absorption at 1.72 THz 86.6% absorption at 3.56 THz [22]. Li introduces a dual-band metamaterial absorber which was designed to operate in the terahertz frequency range. In their work, 0.70 THz absorption bandwidth was obtained where the absorbance was more than 90% [23].

Another important application that is covered in this thesis is sensory applications. Metamaterials have been used as Biosensors, Thin-film sensors, Wireless Strain sensors etc. [24, 25, 26]. Usually, the researchers are working on the sensing application of some previously proposed metamaterial structures. For example, Ben-Xin Wang presented a metamaterial absorber formed by metallic pattern strips and sensory application of that design [27]. In another study, authors used patterned multi-split electric ring resonator with dielectric layer and metallic ground layer. They introduced their sensitivity result for wide-band THz region [28]. The most related three studies to our sensor designs are done by S.J. Park. The authors used classic split-ring resonator and designed a terahertz metamaterial sensor. First, they used their sensor for detecting microorganisms [29]; then,

in another study, they showed the dielectric constant measurements of materials by using their sensor [30]. Lastly, they detected viruses using the nano-gap at the center of the resonator [31].

Active tunability can be achieved in two ways; one is by altering the shape of resonators and the other one is changing the surface response by adding micro-electrical circuit elements to the resonator. After the invention of microelectromechanical systems (MEMS), microelectromechanical actuators were applied to reconfigure metamolecules [32]. Subsequently, the systems were integrated to THz metamaterial by using split ring resonators for tuning the electromagnetic response of the metamaterial [33, 34]. The other method for tuning metamaterials is the, tuning by taking advantage of the nonlinear response of lumped elements integrated into metamolecules. This application was first presented theoretically by Zharov [35, 36], and later, the experimental studies are done by Shadrivov [37].

The last application that is going to be reviewed is metamaterial switches. Switch property can be achieved by integrating superconductors or semiconductors to the structure. Replacement of metallic parts with superconductors gives the ability to manipulate electromagnetic response [38, 39] and also, Embedding photoconductive materials like silicon or graphene to metamaterials are also giving ultrafast switching ability [40, 41].

CHAPTER 2: SIMULATIONS, DESIGNS AND VALIDATION

2.1 Simulations

In this thesis, the objective is to design and analyze two new MTM structures for sub-THz region. To achieve that goal, the designs should be created and analyzed through a computer programme. Accuracy of the results, the completion time of the simulations, data storage and compliance of the programme with the design are the parameters that were important while choosing the proper programme. Finite Integration Technique (FIT) is a simulation method which introduced by Weiland in 1977. The method uses the integral form of Maxwell Equations and enables modeling and analysis of complex structures. The strong side of the program is that the ability to model non-orthogonal geometric objects with cartesian grids [42]. Because of the above properties and the high advantages compared to other simulation methods like Finite Element Method (FEM) and Finite Difference Time Domain (FDTD), FIT method has been employed throughout the whole thesis [43].

The simulations were carried out by finite integration technique based simulation software and for analyzing the frequency dependent absorption of the designed structures, frequency domain solver of this software is used. Proposed designs were aimed to operate with Sub-THz region and in order to achieve that we have run all the simulations within the frequency range between 0.1 THz to 1.0 THz. The boundary conditions were chosen such a way to apply vertically polarized electric field (E_y) and Horizontally polarized magnetic field (H_x) through a transverse electromagnetic mode. Along the z-axis open boundaries are used and the propogation direction of the electromagnetic waves is choosen as z direction throughout whole thesis.

The accuracy of the results is strongly depended on the mesh properties of the simulation. The designs in the simulations are divided by software in to smaller pieces that are called Mesh. The software allows user to select the mesh type and mesh density. It is important to know that higher mesh density will increase the consistency and accuracy of the results. Through whole thesis tetrahedral mesh with the adaptive mesh refreshment are used. The sufficient mesh density is adjusted by adaptive mesh refreshment, and the best results can be gathered. The number of generated mesh cells are also increased by adaptive mesh refreshment until the difference between the results become smaller than the defined accuracy level. The accuracy level for the adaptive mesh density is set to be 1×10^{-6}.

2.2 Designs

2.2.1 Methodology of the Designs

After selecting the boundary conditions and frequency range from the simulation software, the design part is started, and the first thing to do is the selection of the right materials for the design. The materials are the most important part for a metamaterial because the perfect absorption and also the resonance conditions are provided with the impedance match, which is strongly dependent on the properties of the materials like conductivity and permittivity. While selecting the materials, there are some conditions that we should consider one of them is, if the material is abundant in nature. The other important parameter is the side effects of the selected material, it should not harm humans and environment. Lastly, the metarial's costs should be realistic for manufacturing, most of the cases, the design can be perfect via the simulation and analysis process but it is not possible to produce that structure because of the high manufacturing cost. In our case, we

took all these parameters in to account, and decided on the materials that is used in this thesis. After deciding the materials, the material information are needed to be introduced to simulation software. Optical and electromagnetic properties of the materials are derived by the frequency, therefore some frequency dependent constants needed to be defined manually according to frequency range [44]. In the thesis, for some parts, frequency dependent values are introduced to simulation programme manually, these values are taken from literature and referenced in the related chapter.

Following step is to determine the dimensions of the metamaterial structures. As it is mentioned before the lateral dimensions have to be smaller than the wavelength of incoming radiation [45, 46]. For metamaterials, perfect absorption takes place when the impedance of the absorber, z(w), matches with the impedance of the free space which ensures the zero reflection and transmission of the incident wave [47, 48]. Therefore, the geometrical dimensions of the metamaterial structure have a very critical role in determining the response of metamaterial [49]. Roughly the metamaterials usually shows their resonance when the dimensions are usually at 1/10 of the wavelength. For Sub THz regime the corresponding wavelength is between 3 mm to 0.3 mm which indicates that the dimensions should be around 300μm [50].

2.2.2 Complimentary H shaped Fishnet Metamaterial

The fishnet structure is combination of two metal plates with a dielectric in a sandwich form which perforated by small holes and the structure has been extensively studied in recent years [51, 52, 53, 54, 55]. Different from the planar arrays of split-ring resonators,

fishnets can achieve the negative refractive index by exhibiting negative permittivity (ε) and negative permeability (μ) at the same time which is a required property for perfect lenses and many other applications.

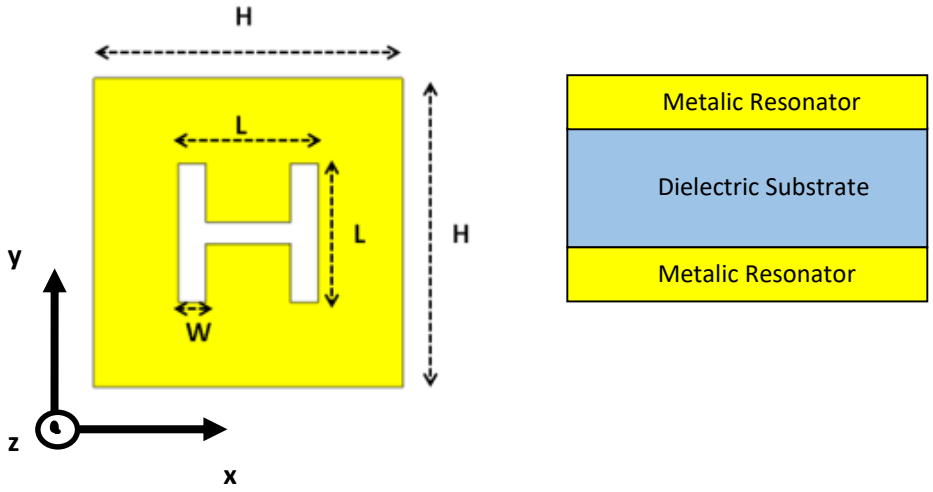

Figure 2-1 Front view and side view of proposed structure

The front view and side view of the proposed structure can be seen from Figure 2.1 There is a H shape gap at the center of the resonator. The width (w) of the H shape is 35 μm and it has 180 μm lengths (L) in both x and y axis. One side of the metallic square resonator is 400 μm. Gold is used for metallic resonator and polymide is used for dielectric substrate and the thickness of the back and front gold plates are 0.3 μm, for the polymide substrate the thickness is set to 15 μm

2.2.3 Terahertz Metamaterial Absorber Comprised of H-Shaped Resonator within Split-Square Ring

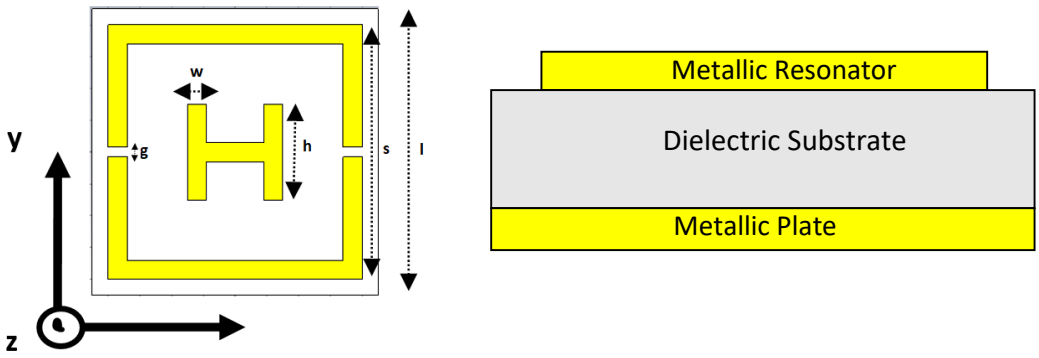

Figure 2-2 Front and side view of proposed MTM structure

The design was chosen in a way that to give the best resonant frequency to incoming electromagnetic wave. In Figure 2.2 the proposed unit cell of the structure is shown. The designed structure consists from three parts; metallic resonator at the top, dielectric material at the center and a back layer metallic plate that covers the whole surface. In this structure the resonator has been designed with combination of two shapes. At the outer part there is a square ring resonator with two gaps at the middle sides and inside the square H shape structure is situated. Gold was used for resonator and the back layer, and for dielectric layer between the resonator and back layer, Polymide was used. The dimensions are very important for the design to give the highest response to incoming electromagnetic wave. The dimensions are given below

The Polymide dielectric layer has square shape with 450 μm side length (l) and the thickness of substrate is 23 μm. For square with gab, one side of square is 400μm (s) and

the width of this square is 30μm(w). The gaps are situated at the center of both right and left side of the square and the gap width is 15μm (g). The H shape at the middle has 150 μm (h) lengths on both y-axis and x-axis and the width of the H shape is 30 μm(w). For the resonator (Square with gap and H at the middle) the thickness is 0.3 μm. The dimensions were chosen after several simulations and the chosen values were the best ones for the resonant frequency.

2.3 Analyzing Approach

From the simulation software, the output is attained as the scattering parameters (S-parameters). Reflection and transmission coefficients can be obtained by using the acquired S-parameters. Our aim is to analyze absorption, which can be calculated by using transmittance T(ω) and reflectance R(ω). The equation 2.1 shows the relation with frequency dependent Absorbance A(ω), Transmittance T(ω) and Reflectance R(ω). The T(ω) and R(ω) values can be obtained from S-parameters, S_{11} represents the reflection, and the absolute square of that value ($|S_{11}|^2$) gives the reflectance in accordance to this, S_{12} represents transmittance, and absolute square of that value ($|S_{11}|^2$) gives transmittance. For absorber metamaterial with a metallic back layer, the transmission is eliminated so we can ignore the transmittance from the equation and the final equation can be shown with Equation 2.3 [56, 57].

$$A(\omega) = 1 - R(\omega) - T(\omega) \quad (2.1)$$

$$A(\omega) = 1 - R(\omega) \quad (2.2)$$

$$A(\omega) = 1 - |S_{11}|^2 \quad (2.3)$$

2.4 Validation

2.4.1 Validation from Literature

In that part, the results of simulation software are compared with a study from literature that is experimentally verified. Shen at al. proposed a triple-band metamaterial absorber which has three absorption peaks at 0.5, 1.03, and 1.71 THz and they experimentally proved their results [58]. The authors used FIT based software for simulations, which is the same for this thesis and then they carried out experimental characterization. The absorber design consists of three layers, resonator, a dielectric layer and a back metal plane. The schematic representation of the design is given in Figure 2.3. For the resonator, the authors combined three different sized concentric square ring with the dimensions w1 = 84 μm, w1 = 56 μm, w1 = 36 μm. Aluminium is used for metallic parts, and polyamide is used for 7.5 μm dielectric layer. The thickness of the aluminium back metal plane and the resonator is 0.2 μm.

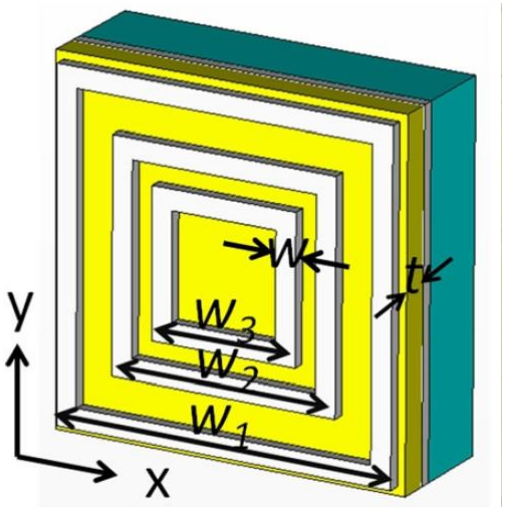

Figure 2-3 Schematic shown of triple-band metamaterial absorber [58]

The same structure is designed from our simulation software, and periodic boundary conditions are used for a unit cell in x and y directions, matched boundary conditions are applied along the z-direction. As a mesh type, tetrahedral mesh with the adaptive mesh refreshment are used. A=1-T-R obtains the Absorption (A). The gathered results are compared with the results of the study and shared in Figure 2.4.

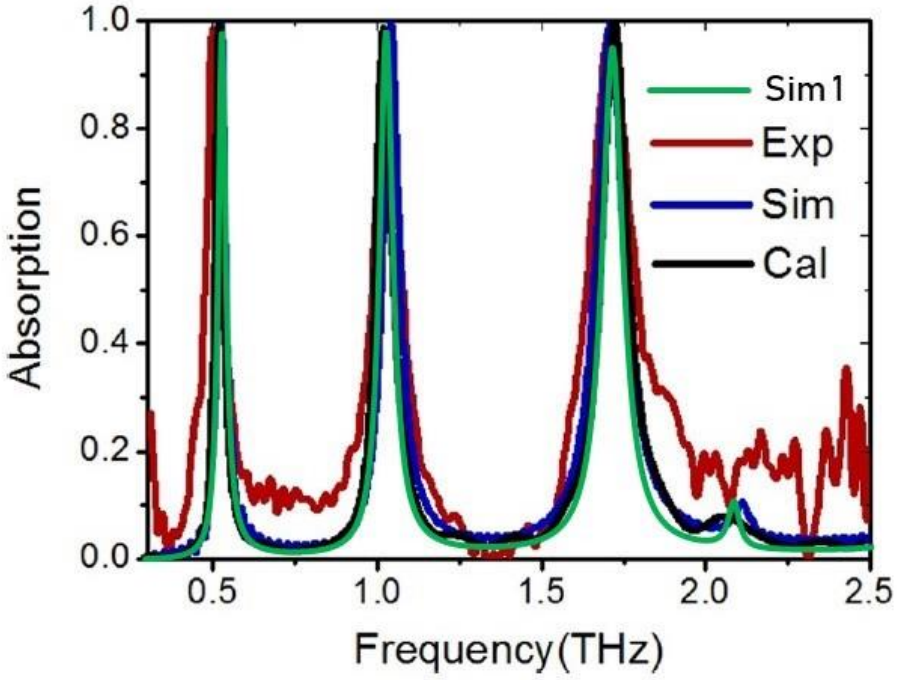

Figure 2-4 Comparison of absorption curves of triple-band metamaterial absorber

From Figure 2.4, our simulation results are shared with the yellow line (Sim 1), and it well matches with the previous simulation (Sim), experiment (Exp) and calibrated (Cal) results of the study. Form the result it can be concluded that the simulation results well matches with the experiment.

2.4.2 S-Parameter Retrieval

For a material, permittivity, permeability, and conductivity are the key parameters to define the electromagnetic characteristics of the structure. The response of a material to an incoming electromagnetic wave depends on these parameters, because of that we should extract these parameters for each frequency to see whether our material is left-handed material or not. In this chapter, permittivity (ε) and permeability (μ) values will be extracted from the refractive index (n) and impedance (z) of the material. First, to find n and z, we need to find S parameters. After the design of our metamaterials, we assigned the appropriate boundary conditions, from ports THz waves were sent, and the S parameters are extracted. In the figure 2.5, we can see the illustration of reflected and transmitted waves from our metamaterial unit cell. From figure 2.5 a. We can see the normal incident wave to a metamaterial slab, however, it is almost impossible to simplify the refractive index of that metamaterial because it is the combination of two different materials and the geometries and thicknesses of that materials will affect the total refractive index and impedance. We can consider our metamaterial as a homogeneous slab, as shown in Figure 2.5 b. And with using the S parameters that are gathered from our simulation, we can calculate the desired parameters.

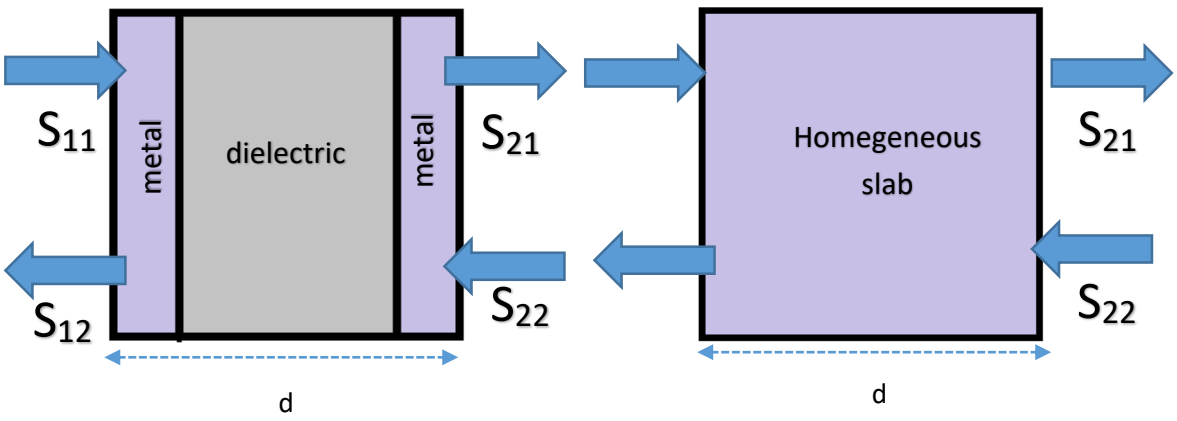

Figure 2-5 Representations of scattering parameters through real design and homogeneous assumption

First we can write reflection coefficient (r) and transmission coefficient (t) in terms of z and n.

$$r = \frac{z - z_0}{z + z_0} \tag{2.4}$$

$$t = e^{jk_0 nd} \tag{2.5}$$

Than we can write S_{11} and S_{21} in terms of reflection and transmission coefficients with using equation (1) and (2), in that equation $k_0$is the wavenumber; d is the maximum length of the structure.

$$S_{11} = \frac{r(1 - t^2)}{1 - r^2 t^2} \tag{2.6}$$

$$S_{21} = \frac{t(1-r^2)}{1-r^2t^2} \tag{2.7}$$

Solving equations (4) and (4) by using the reflection and transmission coefficient values from equation (1) and (2) will give us the impedence (z) value.

$$z = \pm\sqrt{\frac{(1+\mathrm{S}_{11})^2 - \mathrm{S}_{21}{}^2}{(1-\mathrm{S}_{11})^2 - \mathrm{S}_{21}{}^2}} \tag{2.8}$$

And also we can get t value as;

$$t = \frac{S_{21}}{1-S_{11}r} \tag{2.9}$$

Now the last unknow value is refractive index, with using t value which is found from equation (6) and equation (2), we can find the imaginary n″ and the real n′ value of refractive index.

$$t = e^{jk_0(n'+jn'')d} \tag{2.10}$$

$$\ln t = \ln\left(e^{jk_0 n' d}\right) - \ln\left(e^{-k_0 n'' d}\right) \quad (2.11)$$

$$\ln t = j(k_0 n' d - 2\pi m) - k_0 n'' d \quad (2.12)$$

Which m represents the branch coming from the sinusoidal function. At the end from equation (9) we can get real part of n as;

$$n' = \frac{1}{k_0 d}(Im[\ln t] + 2\pi m) \quad (2.13)$$

$$n'' = \frac{1}{k_0 d} Re[\ln t] \quad (2.14)$$

Now we can use the extracted impedance and refractive index to find permittivity (ε) and permeability (μ). The following expressions show the relation of impedance and refractive index with permittivity (ε) and permeability (μ);

$$\varepsilon = \frac{n}{z} \quad (2.15)$$

$$\mu = nz \quad (2.16)$$

As we can see from the equations, there can be multiple solutions for refractive index and impedance because of the value, which represents the branch of a sinusoidal function. If

the maximum length of the structure is less than the wavelength of the wave, we can eliminate this problem. The metamaterial structure can be seen as passive material that we can appropriately select the branch (m) value.

The complex S-parameters for our metal-dielectric-metal fishnet design are shown in Figure 2.4 (a). The six transmission peaks and reflection minima can be seen from the phase graph in Figure 2.6.a and b. These resonances are situated at 0.38 THz, 0.53 THz, 0.64 THz, 0.76 THz, 0.85 THz, and 0.94 THz. For non-amplifying (lossy) medium, the imaginary part of the refractive index and the real part of the impedance should be greater than zero. From the Figure, we can see that the real part of the impedance shows positive value at the strongest resonant region between 0.60 THz to 0.65 THz.

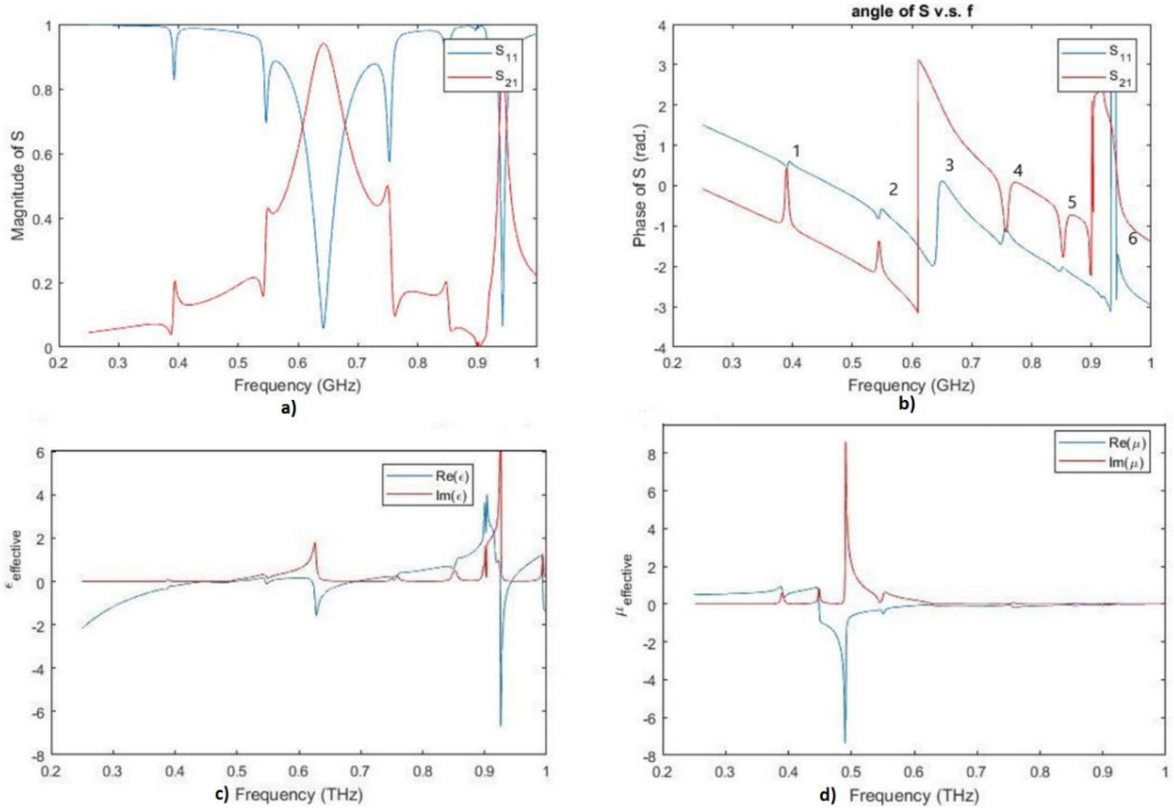

Figure 2-6 S-parameter retrieval results of a) magnitudes b) phase c) real and imaginary parts of effective permittivity d) real and imaginary parts of effective permeability

In Figure 2.6 c effective permittivity values are shared, the real part of effective permittivity is negative between 0.2 THz and 0.68 THz and also at 0.92 THz region which includes the two strong resonances. On the other hand, it can be seen from Figure 2.6.d that real part of negative permeability is below zero between 0.46 THz and 0.65 THz.

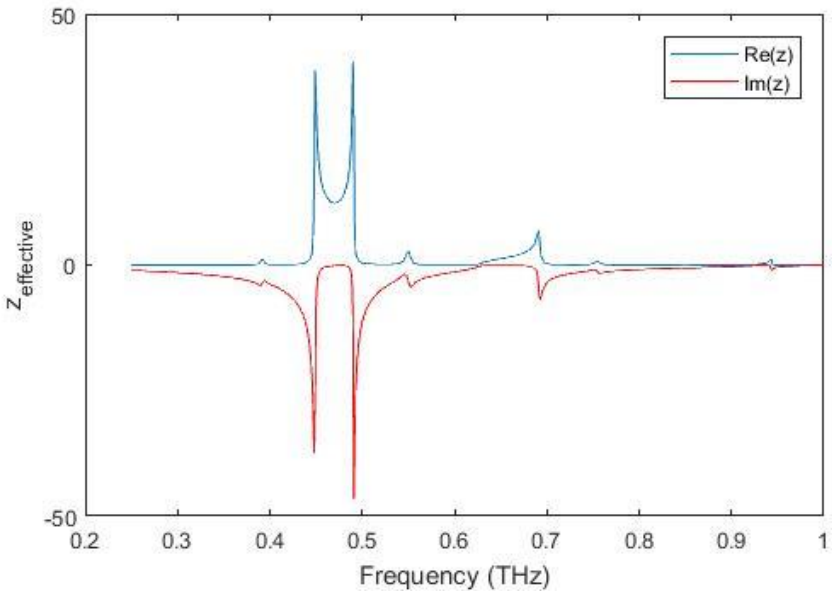

Figure 2-7 Effective impedance of Fishnet structure against frequency

For non-amplifying (lossy) medium, the imaginary part of the refractive index and the real part of the impedance should be greater than zero. From the Figure 2.7, we can see that the real part of the impedance shows positive value at the strong resonant region between 0.55 THz to 0.65 THz. However the refractive index values are not shared with only checking the impedance graph, it can be said that the structure shows left handed material properties.

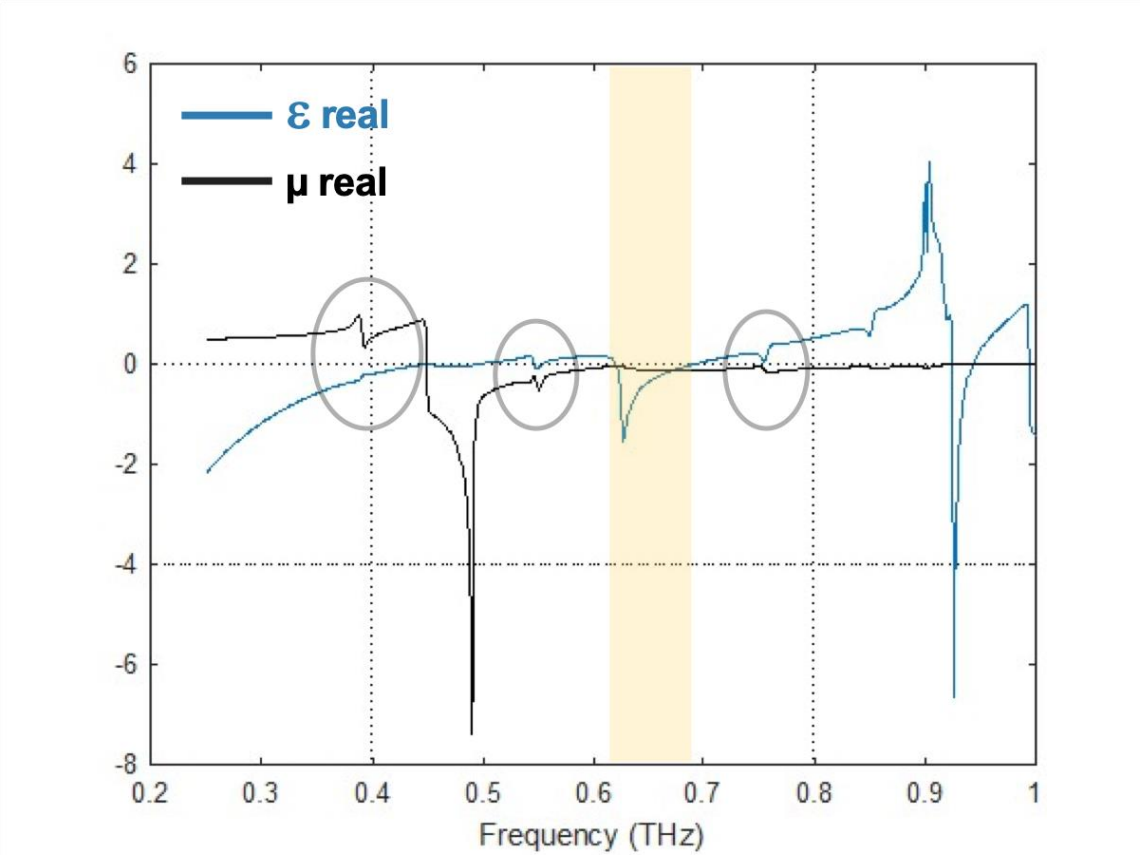

Figure 2-8 Real parts of effective permittivity and permeability via frequency

Real parts of effective permeability and permittivity can be seen together. In Figure 2.6. At the places that are shown with the circles have jumps in permeability and dips for permittivity which indicates double negative media characteristics. With yellow colored region we can see the negative index region. The real part of permittivity around -2 and the real part of permeability is around -0.2 in magnitude, which indicates that left handed material characteristic is achieved.

CHAPTER 3: SUB-THZ MTM ABSORBER

The superior properties of metamaterials have started to be used as an absorber first by Landy [21]. He has introduced the phenomena of impedance match of MTMs with the ambiant air that enables minimum reflection which also means maximum absorption. After that the first THz absorber with 70 % absorptivity was presented by Tao in 2008 [20]. Subsequently the attention moved to producing wide band THz absorber. However the studies are insufficient to fill the Sub-THz region (0.1-1 THz) [58, 59]. In this chapter absorption characteristics of two unique designs are analyzed and their electromagnetic responses are described by using electric field and surface current distribution graphs.

3.1 Complimentary H Fishnet

After designing the proposed structure, the electromagnetic response of the purposed structure is analyzed. It can be realized from Figure 3.1 that at 0.642 THz and at 0.942 THz strong resonances are situated. At these resonant frequencies the impedance of the structure matches well with the impedance of free space and the reflection values are minimized.

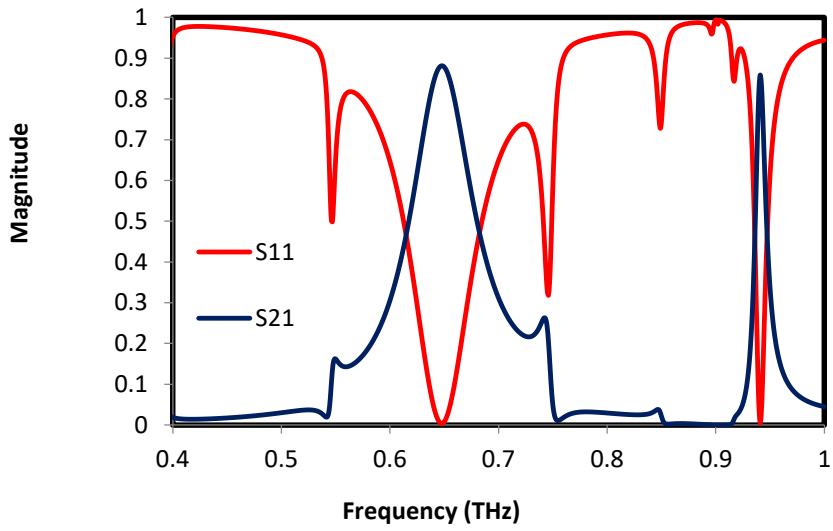

Figure 3-1 Reflection and transmission curves in magnitude for fishnet metamaterial structure

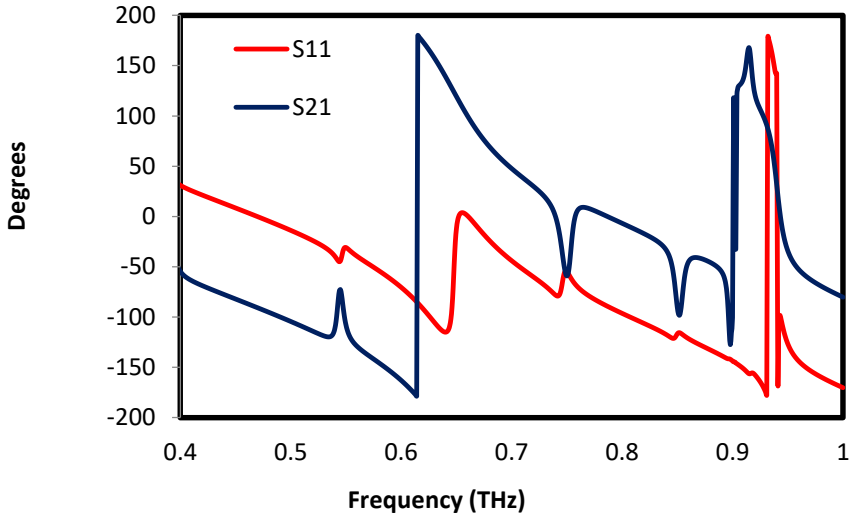

Figure 3-2 Reflection and transmission curves in phase for fishnet metamaterial structure

For understanding the physical characteristics of the resonance frequencies, we examined the electric field and surface current distributions of the proposed MTM fishnet structure. Electric field distributions and surface current distributions are presented for

0.642 THz and 0.942 THz resonant frequencies in Fig 3.3 and Fig 3.4, respectively. For the first resonant frequency the fields are allocated at the right and left sides of the H shape inside the dielectric substrate. For the second resonant frequency electric fields are allocated widely at the right and left side of the whole structure inside the dielectric substrate. As it can be seen from the Figure 3.3 a) strong electric fields around the H shape especially for the first resonant frequency induce surface charges which produce surface currents [60].

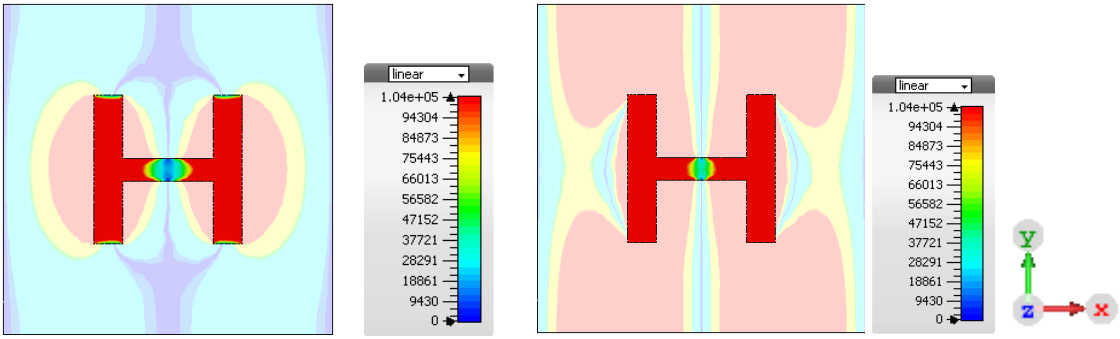

(a) (b)

Figure 3-3Electric field distributions for a) 0.642 THz resonant frequency b) 0.942 THz resonant frequency

In Figure 3.4, we can see the electric field distributions at the inside and outside of the structure. The screen shots of the electric field were taken as we moved along the y-axis. For the resonant frequency at 0.642 THz it can be seen that two intense electric field hot spots are located at the complimentary H structure and the electric field is higher at the middle. The second maxima resonant frequency is shown in Figure 3.4 b The electric field distributions around the complimentary H are weaker than the other resonant but in that

case we can mention about quadrupole interactions with the help of electric fields at the outer of the structure [61].

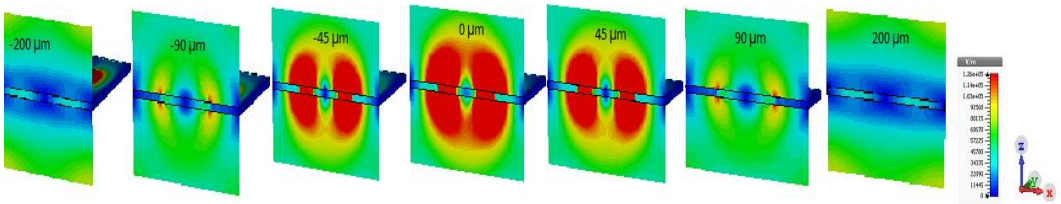

(a)

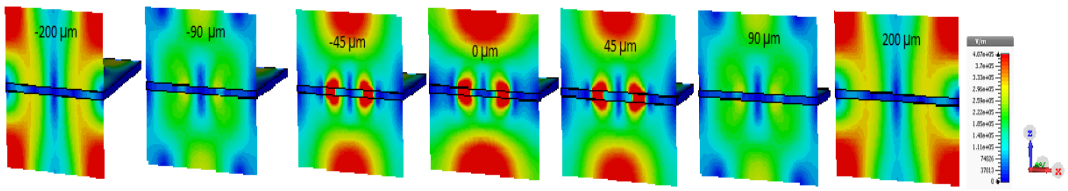

(b)

Figure 3-4 Electric field distributions for resonant frequencies. Pictures plotted in (x-z) plane a) for 0.642 THz b) for 0.942 THz

Surface current distributions for first resonant and second resonant frequencies are given in Fig 3.5.a and Fig 3.5.b respectively. The parallel and anti-parallel surface current distributed around the sides of H shape. For the first resonant frequency the currents strongly concentrated at the upper and down sides of the H shape. Between the left and right side, they show parallel directions. The parallel currents control the electric response and the anti-parallel currents control the magnetic response. If we compare two resonant frequencies, surface currents are stronger for the first resonance frequency, this shows that the impedance of the structure matches with the impedance of free space ($z(\omega)=z_0(\omega)$) [62, 63].

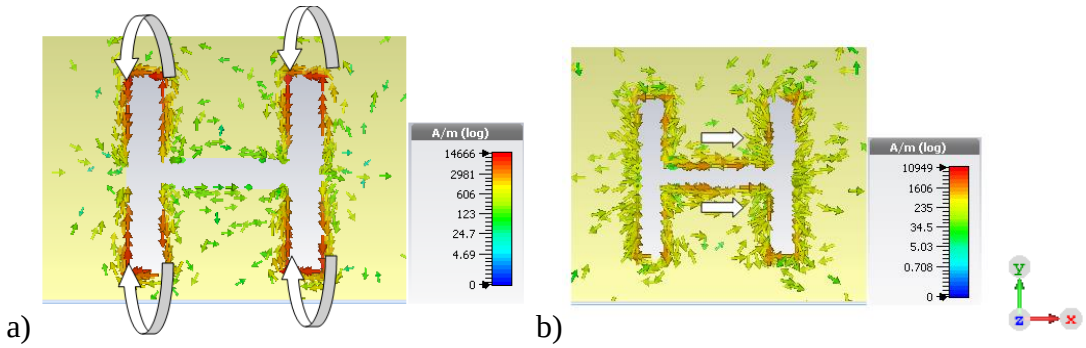

a) b)

Figure 3-5 Surface current distributions for a) 0.642 THz resonant frequency b) 0.942 THz resonant frequency

3.2 Complimentary H Absorber

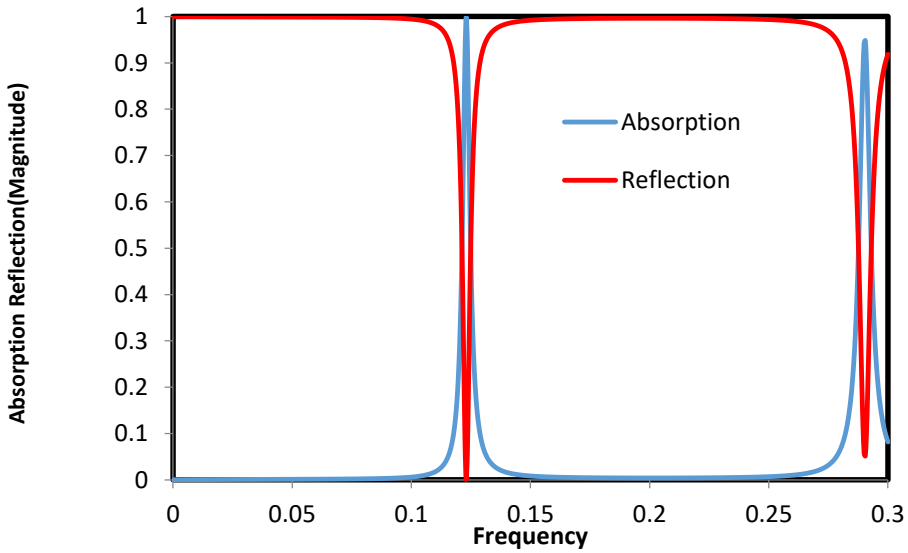

Figure 3-6 Resonance frequencies of the structure

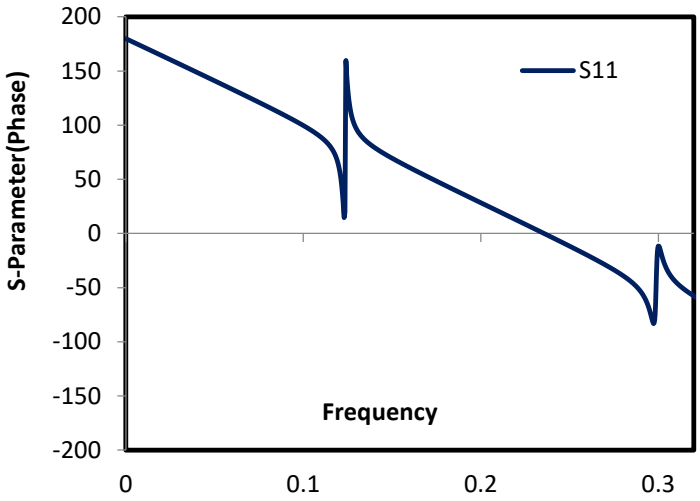

Figure 3-7 Resonance frequencies of the structure

After modelling the structure, the reflection characteristics of the resonator was monitored. The results are gathered from finite integration technique software simulations and periodic boundary conditions are used for a unit cell in x and y directions, matched boundary conditions are applied along z- direction. The absorption (A) is obtained by $A = 1 - T - R$ and transmission is considered as zero where the skin depth of back layer materials is much lower than the thickness of material (2 μm). In Figure 3.6 we can see two resonance frequencies at 0.12 THz and 0.29 THz. By using inductance and capacitance of the structure we can define the resonant frequencies of the structure. In the first resonance frequency at 0.12 THz 99.9% absorption is achieved which is classified as a perfect absorber and at 0.29 THz the absorption is 91.8%. Because of the high absorption rate in the first resonance frequency we used this frequency in our sense testing steps.

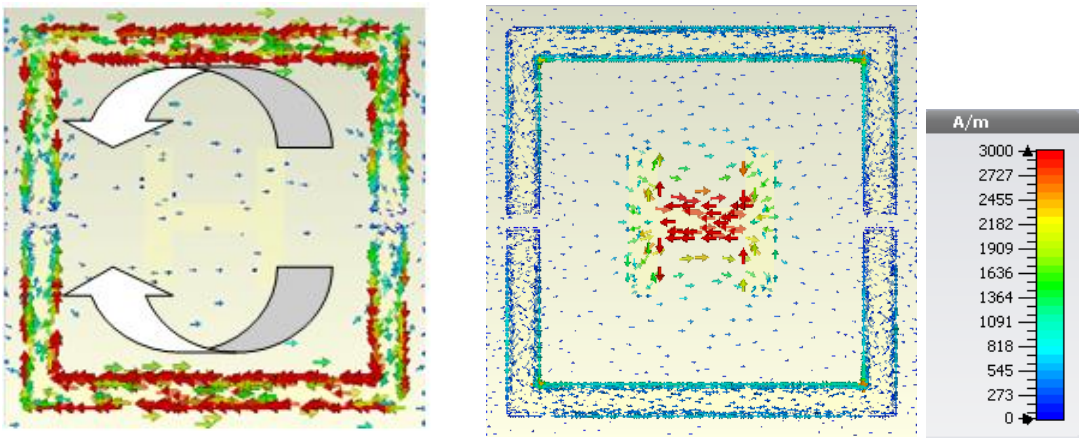

(a) (b)

Figure 3-8 a) Surface current distributions at 0.123 THz b) Surface current distributions at 0.290 THz

The resultant surface current distributions on the resonator are shown in Figs 3.8, a and b respectively for the two resonant frequencies at 0.12 THz and at 0.29 THz. In Fig 3.8.a, it can be seen that for the 0.12 THz frequency, the surface current flows in clockwise direction for the down side of the outer square ring and anti-clockwise direction at the upper side of the outer square ring. At the sides of the outer square by the effect of gaps the opposite current direction can be seen. For the frequency at 0.29 THz, the resultant surface current flows at the center H shape structure and at the outer square the current flow is weaker. From these figures we can say that the effect of outer square ring is higher for the first resonance frequency and the inner H shape is responsible for the second resonance frequency.

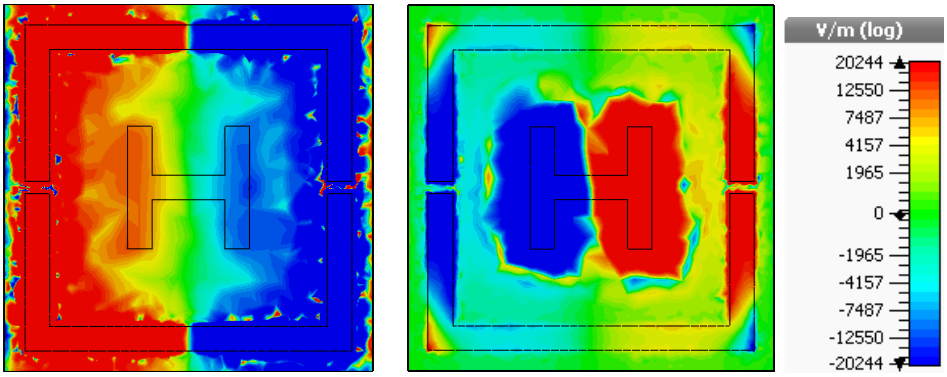

(a) (b)

Figure 3-9 Electric field distributions (a) for the resonance frequency 0.12 THz (b) for the resonance frequency 0.29 THz

Figure 3.9 shows the Electric field distributions on the surface of the structure at resonant frequencies. At the left side the electric field distribution at the frequency 0.12 THz can be seen and at the right side we can see the electric field distribution at 0.29 THz. Likely to surface current distribution it can be seen that the outer square is responsible for the first resonance frequency and the inner H shape is the source of second resonance frequency.

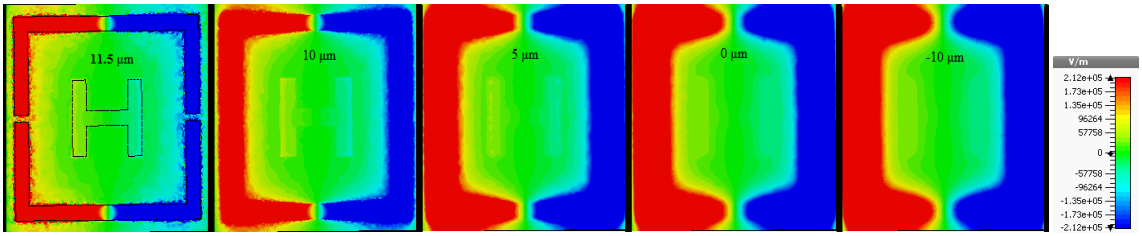

Figure 3-10 Electric field distributions inside the dielectric substrate at 0.12 THz resonant frequency

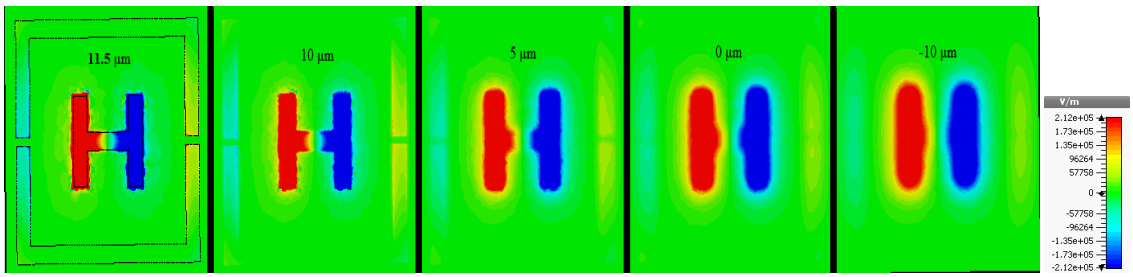

Figure 3-11 Electric field distributions inside the dielectric substrate at 0.29 THz resonant frequency

From Figure 3.10 and 3.11 we can see the electric field distributions inside the dielectric substrate for the 0.12 THz and 0.29 THz resonant frequencies respectively. If we compare these distributions with the ones in Fig. 6 we can see that the two dipoles which come from the outer square and H shape at the middle are disappearing when we go deeper inside the dielectric substrate. For the 0.12 THz resonant frequency we can say that the distributions mainly focused on the right and left sides of the outer square, especially at the regions close to back layer metallic plate. However, for the 0.29 THz resonant frequency the distributions start to focus on the right and left sides of the H shape.

3.3 Conclusion

In this chapter the absorber characteristics of the structures were analyzed. First we analyzed the reflection and transmission characteristics of the proposed structures. After choosing the maxima resonant frequencies, electric field and surface current distributions are analyzed in order to understand the physical characteristics of the proposed fishnet and Complimentary H absorber metamaterial structures. 97.3% and 99% absorption rates were achieved for fishnet and Complimentary H absorber MTM structure respectively.

CHAPTER 4: ABSORBER AND FISHNET SENSOR

In the previous part, with the assistance of our unique design we gathered good absorption values for Sub-THz region which is between 0.1 to 1 THz. In this chapter metamaterial-based absorber and fishnet sensors were tested. MTMs are physically small and with modifying their geometrical parameters, resonant response can be adjusted and that gives them perfect sensing features for chemical and biological applications. The working principle of this sensor is to analyze samples by using the resonance shift of the designed structure as a result of interaction between the EM waves and the samples [64, 65]. By detecting the shifts in the resonant frequencies of MTM structures an unknown material can be found. Each material has its own characteristic dielectric constant, with using our proposed sensors when we add the unknown material as an overlayer, the shift in the resonant frequency can be used as a specific sign for finding dielectric constant of that material. Also thickness of a material can be found by using these resonant shifts [66, 67].

4.1 Complimentary H Absorber Sensor

The proposed metamaterial absorber is used as a sensor in this section. Because of the high absorption rate in the first resonance frequency we used this frequency in our sense testing steps. An overlayer is added to the structure for assessing the sensing ability of the proposed structure. This overlayer represents the material that is to be detected. For the first step, the dielectric constant and the loss tangent of the overlayer material were kept constant and thickness of the overlayer material has been changed. The dielectric constant was set to 2 and the loss tangent was set to 0.0025. The thickness of overlayer is increased

from 0 μm (which represents the air) to 8μm for analyzing characteristics of sensor device as a function of overlayer thickness. In order to show the shift clearly, even thickness values are used in Figure 4.1. In this Figure the shift of the resonant frequency by the effect of overlayer thickness is shown. From the Figure we can see that the reflection resonance frequencies are down-shifted as the thickness increased. The reason for this down-shifted might be the increase in the capacitance of the structure, when the thickness of the overlayer increases the capacitance of the sensor increases and this cause a down-shift to resonant frequency.

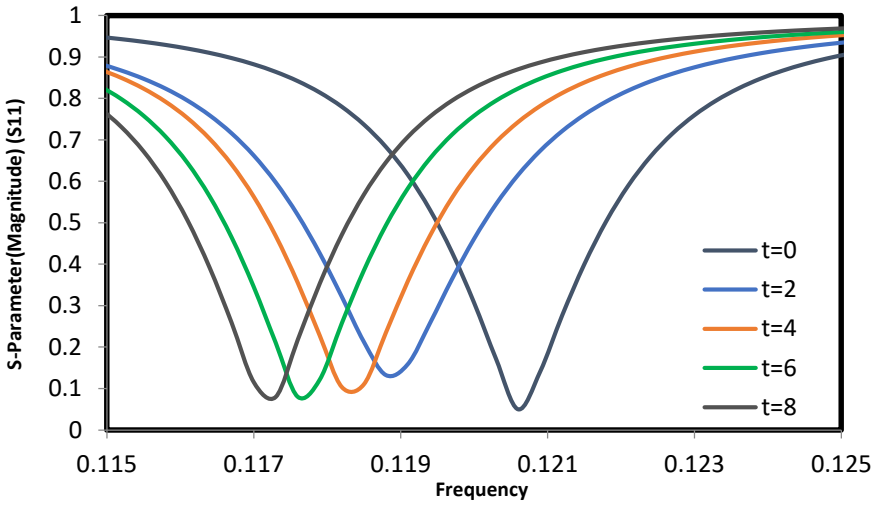

Figure 4-1 S11-parameter of structure with overlayer as a function of varying thickness (t).

Second step is to keep thickness and loss tangent constant and changing the dielectric constant of overlayer material, this process will help us to understand the characteristics of the sensor. For this step, again we looked at the resonance frequencies for reflection. The thickness of the overlayer was kept at 2μm and the loss tangent was kept at 0.0025. The dielectric constant values 1, 2, 3, 4, 5 are used to show the change of reflection

resonance by permittivity. The permittivity value ε=1 shows the dielectric constant of the air. As a result of this simulation it can be seen from Figure 4.2 that the resonance frequency decreases as the permittivity increases. The permittivity value ε=1 shows the dielectric constant of air.

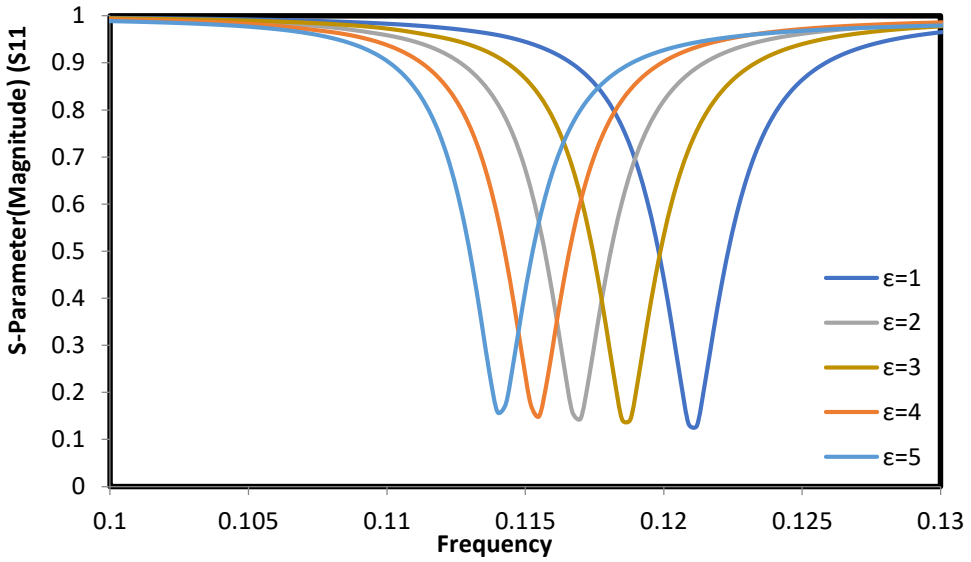

Figure 4-2 S11-parameter of structure with overlayer as a function of varying permittivity(ε).

Afterward, the effect of variation of loss tangent of the overlayer on the reflection resonance frequency is analyzed, for this dielectric constant of the overlayer is set to 2 and the thickness of the overlayer is set to 2 μm. The tangent delta values are chosen in a way that the effect of variation of it can be seen clearly. For the tangent delta values 0.0025, 0.025 and 0.25 the simulations are run and in Figure 4.3 it can be seen that resonance frequencies are not changing but the magnitude of reflections are getting higher while the loss tangent is increased. Different materials have different losses so we can use that curves to detect the material from its own specific loss.

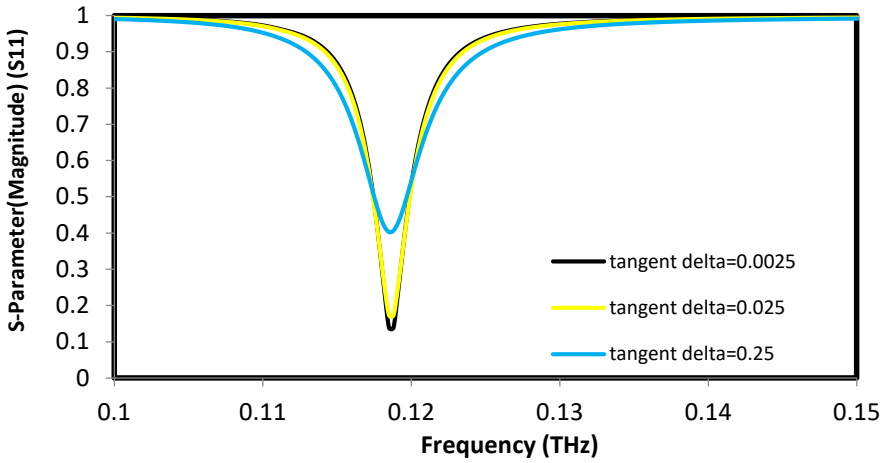

Figure 4-3 S11-parameter of structure with overlayer as a function of varying loss tangent.

Percentage frequency shifts and sensitivity results of the design are given in Figure 4.4. The sensitivity values are calculated from the slope of linear fit lines. It can be seen from the figure that the frequency shift changes are higher for different permittivity values which shows higher sensitivity. However, the sensitivity values are not much high from the literature, they indicate the structure is applicable for sub-terahertz region which is really lack from that kind of devices especially for frequencies less than 0.5 THz.

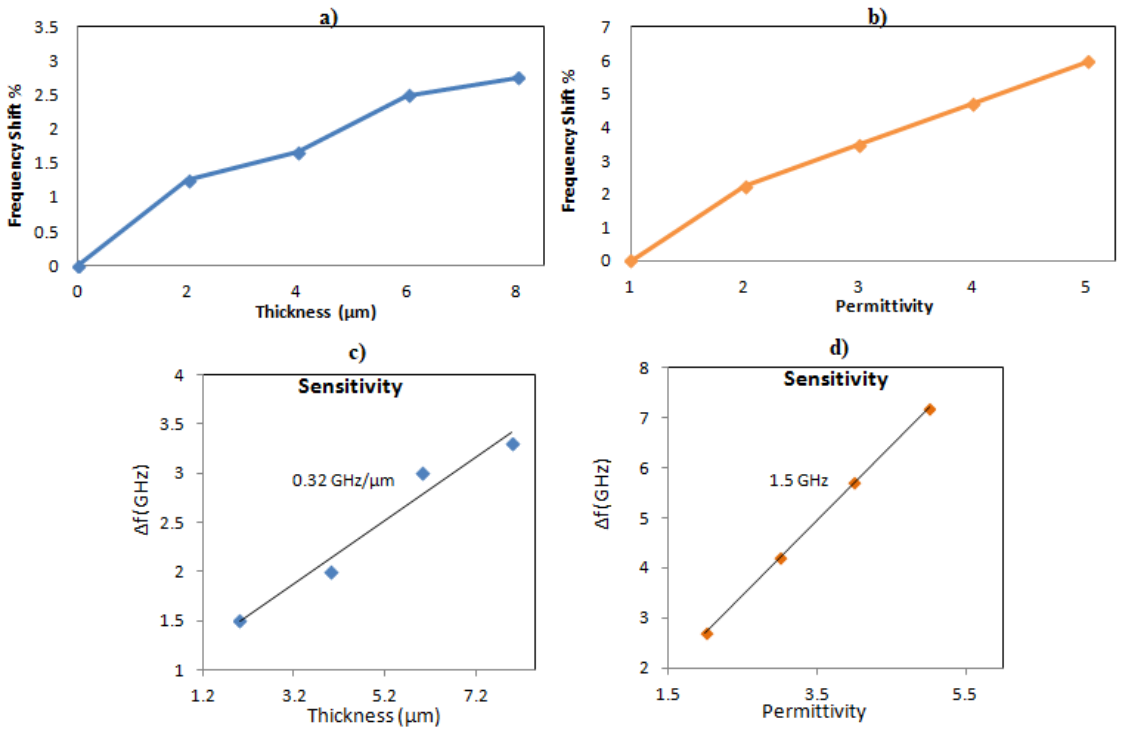

Figure 4-4 Frequency shift percentages against a) Thickness of the overlayer material and b) permittivity of the overlayer material. Sensitivity values c) thickness sensor and d) permittivity sensor

4.2 Fishnet Sensor

(a) (b)

Figure 4-5. a) Single Over-Layer Sensor configuration b) Double Over-Layer Sensor configuration

In this application, two side of the metamaterial structure can be used for sensing purpose. Both front and back side of the structure has a detection system and an unknown material will be integrated as an overlayer (OL). From the change in transmission/reflection characteristics of the detector, the unknown materials can be analyzed. The representation of single and double overlayer fishnet sensors are shared in Figure 4.5 a and 4.5 b respectively.

The response of the sensor is analyzed when the permittivity and thickness of the overlayer (OL) materials are varied. For the first step the thickness of the OL material was set to 2 μm and simulations were run, in Figure 4.6 the shifts in the reflection resonance frequency for single OL sensor by the effect of permittivity can be seen. We can say that while the permittivity of OL material increases the resonance frequency decreases. The reflection curves for double OL resonance frequency is shown in Figure 4.7. The same results like single OL can be seen in this figure, while the permittivity increases the resonance frequency decreases. From the figure, it can be seen that the shifts are wider and this affects the sensitivity of the sensor. As a result of these Figure 9 and 10, we can say that by adding an OL at the back of the sensor, sensitivity of the sensor is increased.

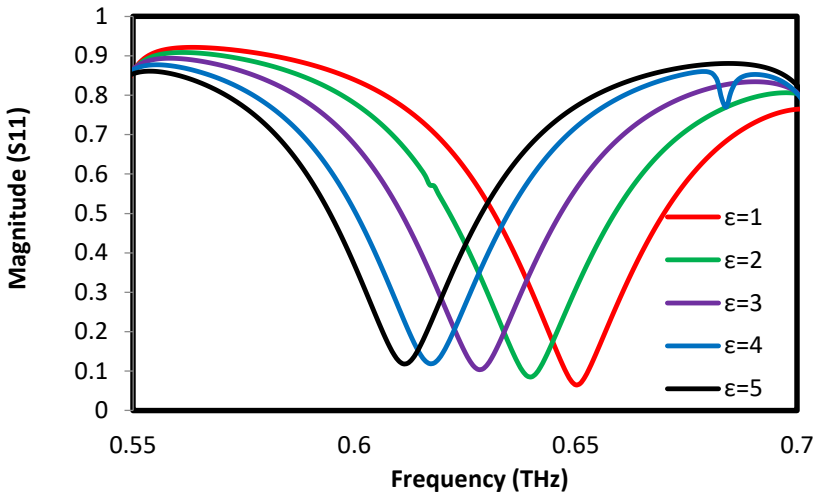

Figure 4-6 Frequency response of the reflection for different single OL permittivities.

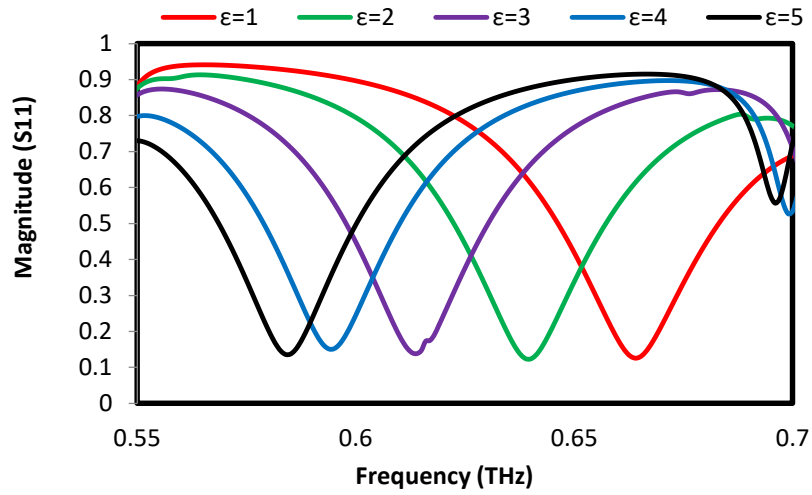

Figure 4-7 Frequency response of the transmission for different double OL permittivities.

For the second step, the permittivity of the OL materials was kept at 2 and the thickness of the (OL) materials was changed and the simulations were run. The reflection curves for single and double overlayers are shown in Figure 11 and Figure 12 respectively. It can be realized from the graphs when the thickness increases, for both single and double

overlayer sensors the resonance frequencies shift to lower frequencies but for double overlayer application we can say that the shift is higher and this gives us high quality of sensing ability.

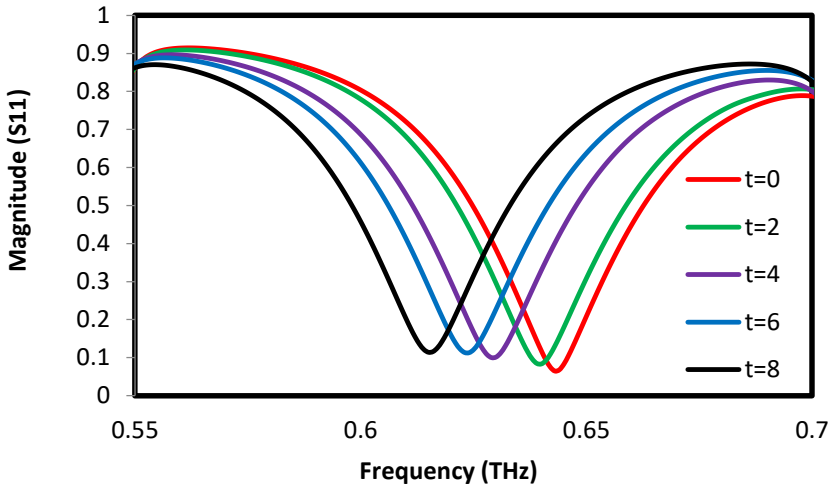

Figure 4-8 Frequency response of the reflection for different single OL thicknesses.

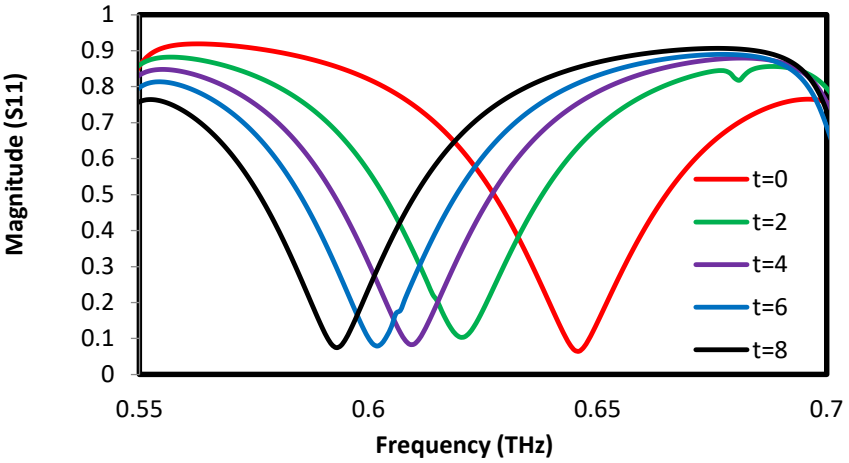

Figure 4-9 Frequency response of the transmission for different double OL thicknesses.

The Figures 4.8 and 4.9 shows the comparison of the frequency shifts in double and single overlayer applications. From the Figure 4.8. it can be seen that for double OL sensors the resonance shifts are almost three times more than the shifts in single OL for different permittivity values. Figure 4.9 shows us that again the resonance shift percentages are higher for double OL applications. From that result it can be concluded that double OL application increases the efficiency of the sensor however for some substances it is not possible to sense by two side of the sensor in that case we have to use single OL sensor.

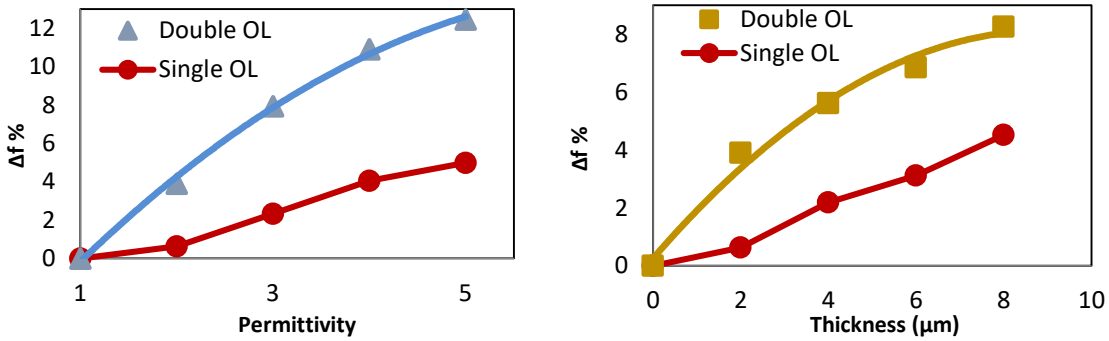

Figure 4-10 a) Frequency shift percentages against different permittivity values for single and double OL b) Frequency shift percentages against different thicknesses for single and double OL

In order to prove the sensing ability of the proposed structure we can compare the sensitivity characteristics of it with the classic split ring resonator sensor. In Figure 4.10 the sensitivity of double and single overlayer sensors are given with respect to varying overlayer thicknesses. The sensitivity values are calculated from the slope of linear fit lines, for double OL sensor the sensitivity is 6.25 GHz/µm for overlayer thicknesses less than 10 µm on the other hand for classic SRR sensor Sabah calculated 5.2 GHz/µm

sensitivity value if the overlayer thickness is less than 5 μm [68]. SRR sensor has sensitivity value of 0.66 GHz/μm for higher overlayer thicknesses from that results we can conclude that our design has higher sensitivity than classical split ring resonator.

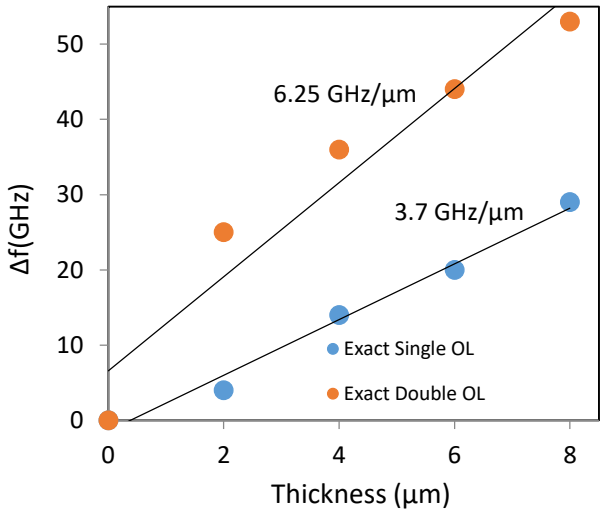

Figure 4-11 Frequency shift of Fishnet MTM versus Double and Single overlayer thickness with the fitted curves.

4.3 Conclusion

In this chapter, a new metamaterial MTM absorber sensor and fishnet sensor which operate at Sub-THz region were investigated, and simulations were run for testing the sensing ability of the proposed structure. Firstly, absorber sensor is designed from the software; the material to be detected is modelled as an overlayer on top of the resonator. Different thickness and permittivity values of the overlayer cause different electromagnetic responses, with using that principle the shifts in the resonant frequencies are investigated against the change in thickness, permittivity and the loss tangent of the overlayer material. These shifts in the resonance frequencies can be used for detecting an

unknown material. Secondly, MTM fishnet sensor is designed and analyzed. The advantage of fishnet sensor is that both sides of the structure can be used as a sensor. Single and double OL were integrated as a material to be detected, and with changing thickness and permittivity of the overlayers, the shifts in resonance frequencies were investigated. As a result of this study, we can say that both proposed structures can provide sufficient detection in the THz region, and they can be used in various applications as a sensitive sensor.

CHAPTER 5: TUNABILITY

5.1 Complimentary H-Absorber Tunability Introduction

Metamaterial absorbers are being used in THz applications widely for their advanced absorption ability, however in some applications traditional MTM absorbers are insufficient because of their fixed operation frequencies. Tunable MTMs are the candidates for filling this gap and they can be used in; active filters, tunable perfect absorbers, electro optical switches, high directional high gain antennas and wide angle beam steering devices due to their wide band ranges. It is known that, an active or adaptive absorption can be achieved by changing the impedance of metamaterial absorber layers in response to applied electrical or optical signal. In the literature there are various studies that are being conducted for tunable metamaterials. There are different methods for tuning metamaterials like alteration of geometry of the resonator, electro-optical tuning, inserting active diodes and so on [69]. Although the numerous number of studies exist for tunable metamaterials, there are few studies that is conducted for THz region. Implementation of active diodes, Micro-Electro-Mechanical Systems (MEMS) and Semiconducting Substrate are the types that have been studied for tuning THz MTMs [70]. In this chapter the tunability of the unique H-shaped Absorber is studied with mechanically with using MEMS and electrically by integrating active diodes.

5.2 Mechanical

5.2.1 Micro-Electronic Mechanical Systems

Mechanical tunabilty can be achieved by geometry alteration of the design. In Micro-Electronic Mechanical Systems the tuning can be made by either changing the split ring size (in our case square ring size) or by creating a new split [70]. The advantages of MEMS can be listed as; it doesn't require any external electrical current, thermal or optical stimuli and these systems can reduce thermal and electromagnetic noise comparing with the other systems.

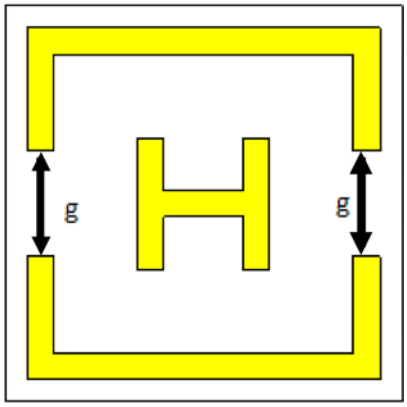

Figure 5-1 Gaps (g) at the sides of the square ring resonator

In Figure 5.1 the gaps on the complimentary H shaped absorber is shown with the letter g. The gaps are making the dipoles on the outer square ring which are responsible for the resonance situation as we discuss in chapter 3, with using electric and current field distribution graphs. Changing the distance of that gap will manipulate the electric field distribution around the gaps and also it will affect the current distributions at the surface. With using micro mechanical systems current technologies allow us to change the gap distance remotely. According to the usage of the absorber, we can change the gap which

means that we can also change the electromagnetic response of the absorber. In figure 5.2 the reflection characteristics of the absorber is given against different gap values.

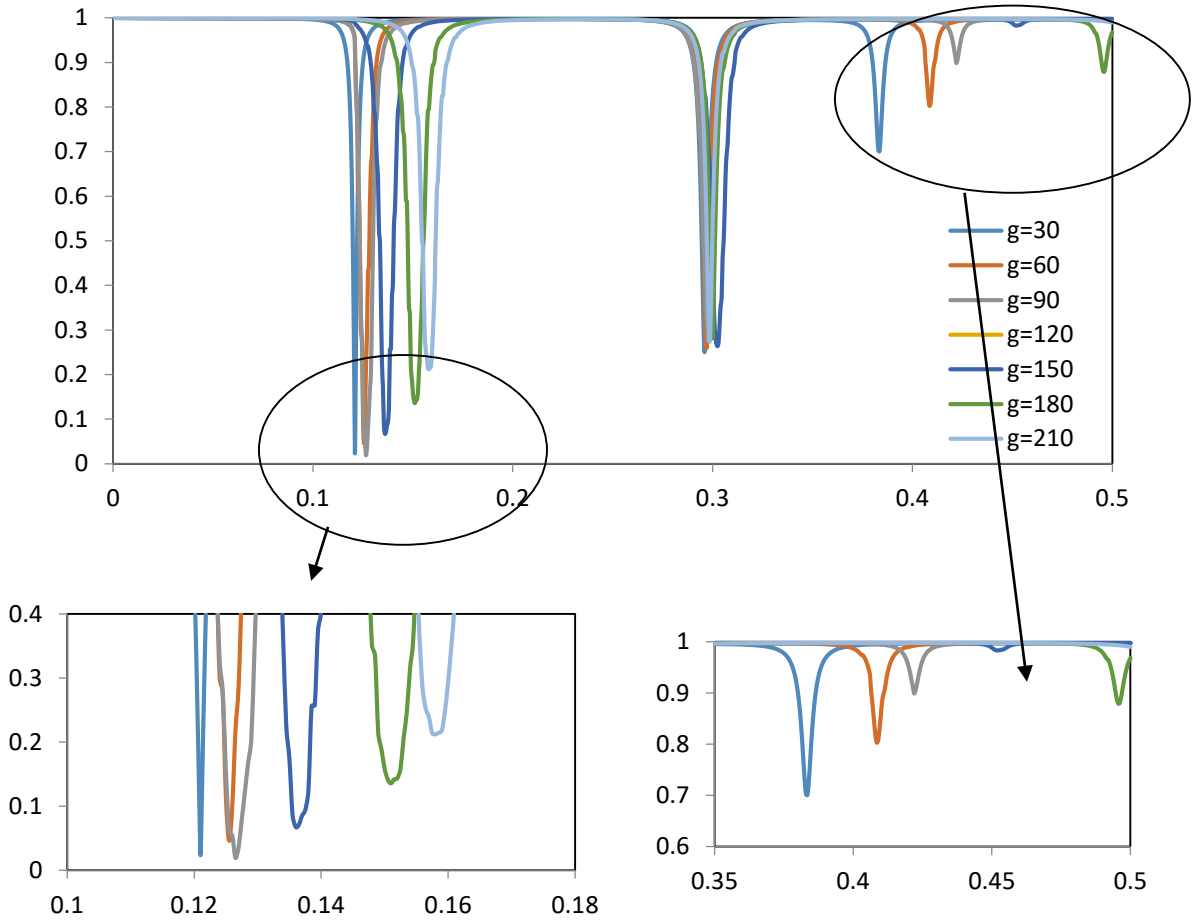

Figure 5-2 S11 parameters for different gap distances.

As it can be seen from the Figure 5.2, the resonance frequencies are tuned by changing the gap distance. With assisting from chapter 3 we know that the outer square ring was responsible from the first resonance frequency, if we check the Figure, it is clear that first resonance frequency is highly tuned while second resonance fluctuation is negligible with compare to first one. In the third resonance the tuning is also significant but the reflection values are pretty high which is not a desired result. We can conclude from the graph that

creating a 200 μm change in the gap will be resulted as 40 GHz shift in the resonant frequency.

5.2.2 Tunability with Changing Orientation

The complimentary H-shaped absorber's resonator is in a non-symmetrical shape, so the electromagnetic response of the structure may change due to the orientation of the structure. This feature can be used for manipulating the resonance frequency. The combined unit cells are illustrated in Figure 5.3 with two different orientations. The Figure 5.3-a represents the combination of four unit cells oriented with the normal phase as it is presented from the beginning of the thesis, beside that Figure 5.3-b illustrates 90 degree rotated form of the same combined four unit cells.

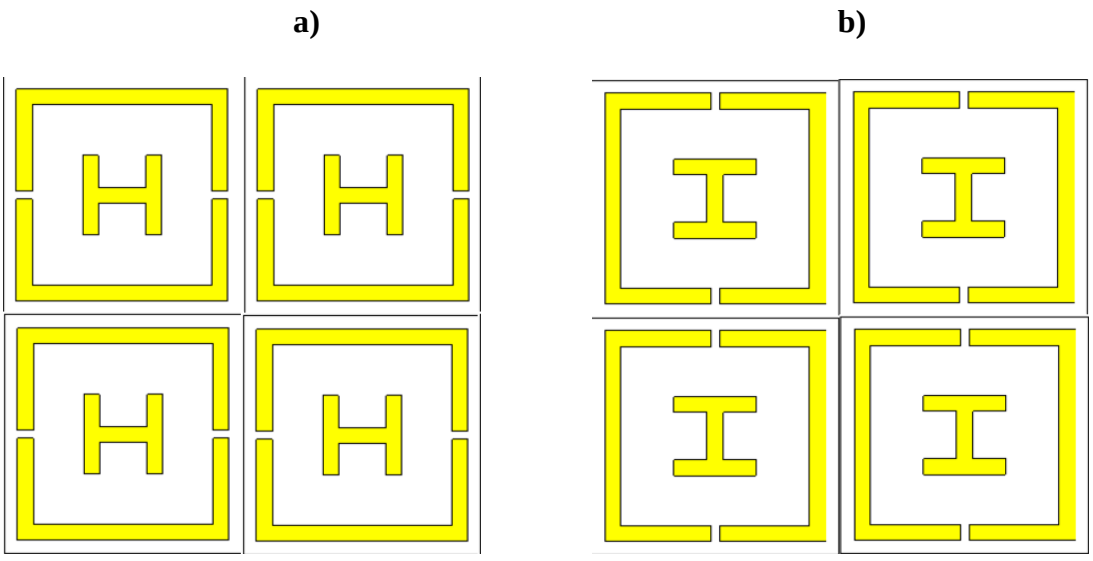

Figure 5-3 Illustrations of combined 4 unit cells a) the normal orientation b) 90 degree rotated form

The electromagnetic response of both orientation is tested by applaying boundary conditions vertically polarized electric field (E_y) and Horizontally polarized magnetic field (H_x) through a transverse electromagnetic mode through the simulation software. The reflection for both orientations are shared in the Figure 5.4 with the magnitudes of scattering parameters S_{11}.

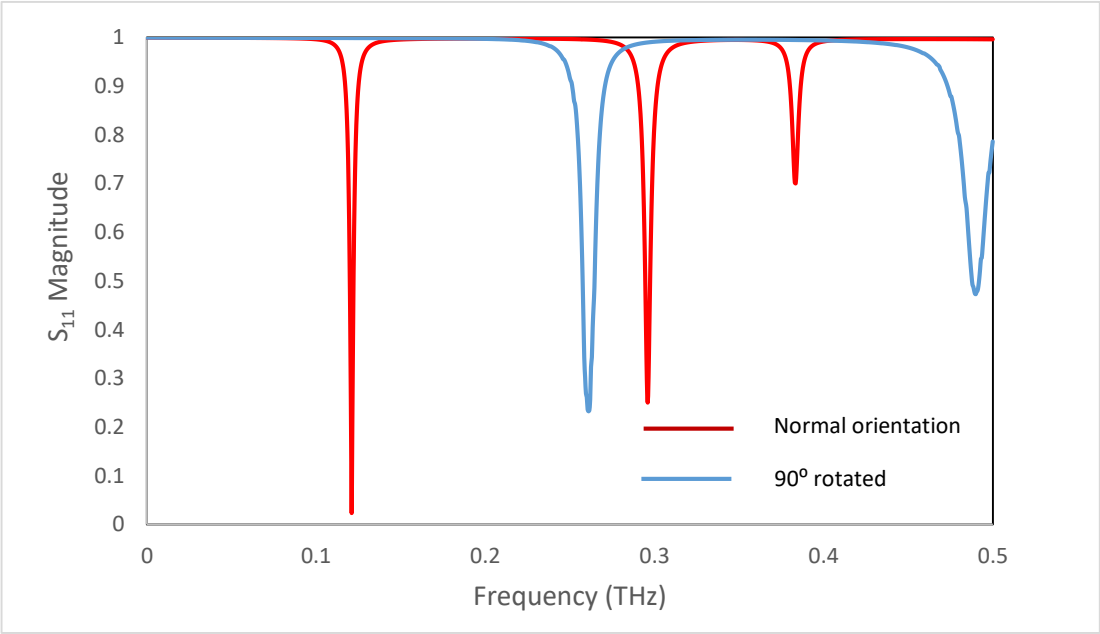

Figure 5-4 S11 parameters of complimentary H absorber with normal and 90^0 rotaded orientations.

Different from the normal oriented unit cell, the 90º rotated unit cell has two resonance frequencies at 0.26 THz and 0.49 THz. Altough the perfect absorption disappears in the rotated design, the noticable changes in the reflection curves confirm that the operation frequencies can be tuned by changing the orientation of the design. As a real application, the design's orientation can be adjusted by mounting it on a remotely rotary surface. Then

the orientation of the planar metamaterial absorber surface will have a selective operation frequeny.

5.3 Electrical

5.3.1 Tunability with Active Diodes

Embedding diodes to the structure is the most common used techniques for tunable MTMs because of their simple integration. The resonant frequency of the resonator can be easily controlled by changing the capacitance and resistance of the active diode through an external stimulation. Varactor and pin diodes have been used in the literature to achieve tunability goal in Radio Frequency range. One of the first tunable MTMs was introduced by Wang et al. [71], they proposed a S-shaped resonator with embedded microwave varactors which they can control the resonance. Filippo et al. [72] presented a tunable varactor diode integrated MTM with an efficient method that can reduce amount of varactors for GHz region. Tennant et al. [73]demonstrated an active frequency selective surface by using pin diodes for controlling unit. They concluded that the proposed structure can be used for tuning the resonant frequency within the range of 9-13 GHz. Recently the focus on tunable MTMs are shifted from microwave region to THz range. With the improvement of technological devices and manufacturing techniques it becomes easier to integrate diodes and other electrical components in to THz metamaterials. Limei et al. [74] designed a tunable THz MTMs absorber with using active diodes. In their study they changed resistance of the resonator by using electrically controlled diode. The resonant frequency changed with the change of meander-line resonator's surface resistance. However, in this chapter an active diode is implemented to the gaps of H-

shaped absorber and both resistance (R) and capacitance (C) of the diodes were changed. In Figure 1. the implemented diodes can be seen at the right and the left sides of the Square Ring Resonator (SRR).

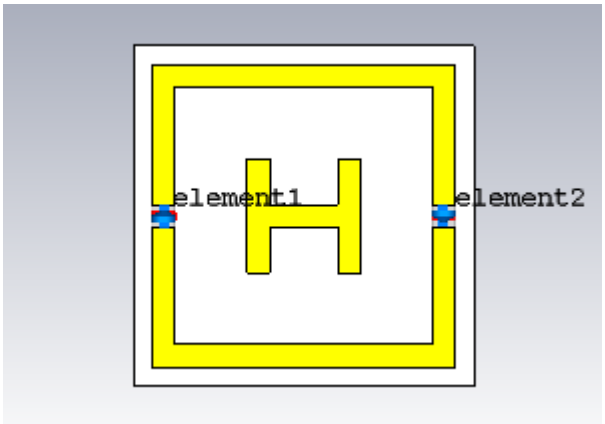

Figure 5-5 Front view of H-shaped Absorber with active diodes

In order to understand the response of the structure to the incoming electromagnetic wave, we can assist from the equivalent circuit of the absorber which is presented and analyzed by other researchers [75, 70]. In Figure 5.5 the transmission equivalent circuit can be seen. The metalic lines on the dielectric substrate act like an inductor (L) and the gaps between metalic lines which are the dielectric substrates can be considered as capacitance (C). Ohmic losses from the surface can be shown by a resistor (R_0) and the R_S represents the variable resistance which is the effect of implemented diodes. At the circuit Z_0 represents the characteristic impedance of the free space and Z_H shows the input impedance of our resonator for perfect absorption the impedence match of free space and proposed resonator should be achieved. With using active diodes which can be controlled by bias-voltage we can change the R_S and C values of our circuit which

will affect the impedance of our resonator. The changes in variable resistor will vary the whole impedence of absorber, then the absorption of the structure will be lower or higher according to the variation of the resistor. On the other hand the relation of capacitor is a bit different, the resonant frequency (w_0) is directly proportional with the capacitance $\omega_0 \sim (LC)^{-1/2}$. So the variation in the capacitance will result with a shift in the resonance frequency.

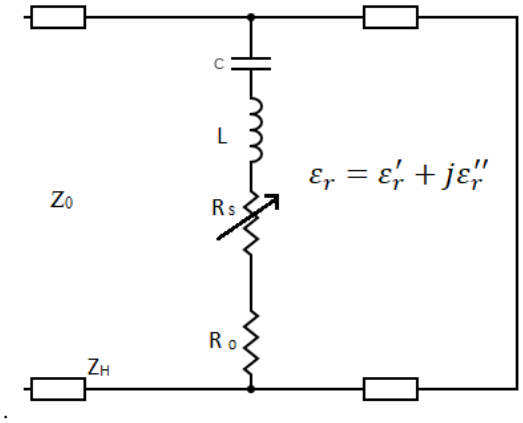

Figure 5-6 Transmission Equivalent Circuit for Absorber MTMs

First, we changed the R values by applying a bias voltage to the diodes and see the changes in resonance frequency. The capacitance of the diode set to 1 pF and the results can be seen in Figure 5.7 as the effect of SSR and inside H-shape is described in chapter 3 with using the current field and electric field distributions. However, we analyzed that SRR effect is mostly on the first resonant frequency we can see from the Figure 5.7 that only the magnitude is changing by the R values while ω_0 keeps at a constant value, but for the second resonant, we can see the shifts in ω_0 value. The interactions between the outer ring and inside H-shape affects the impedance of resonator.

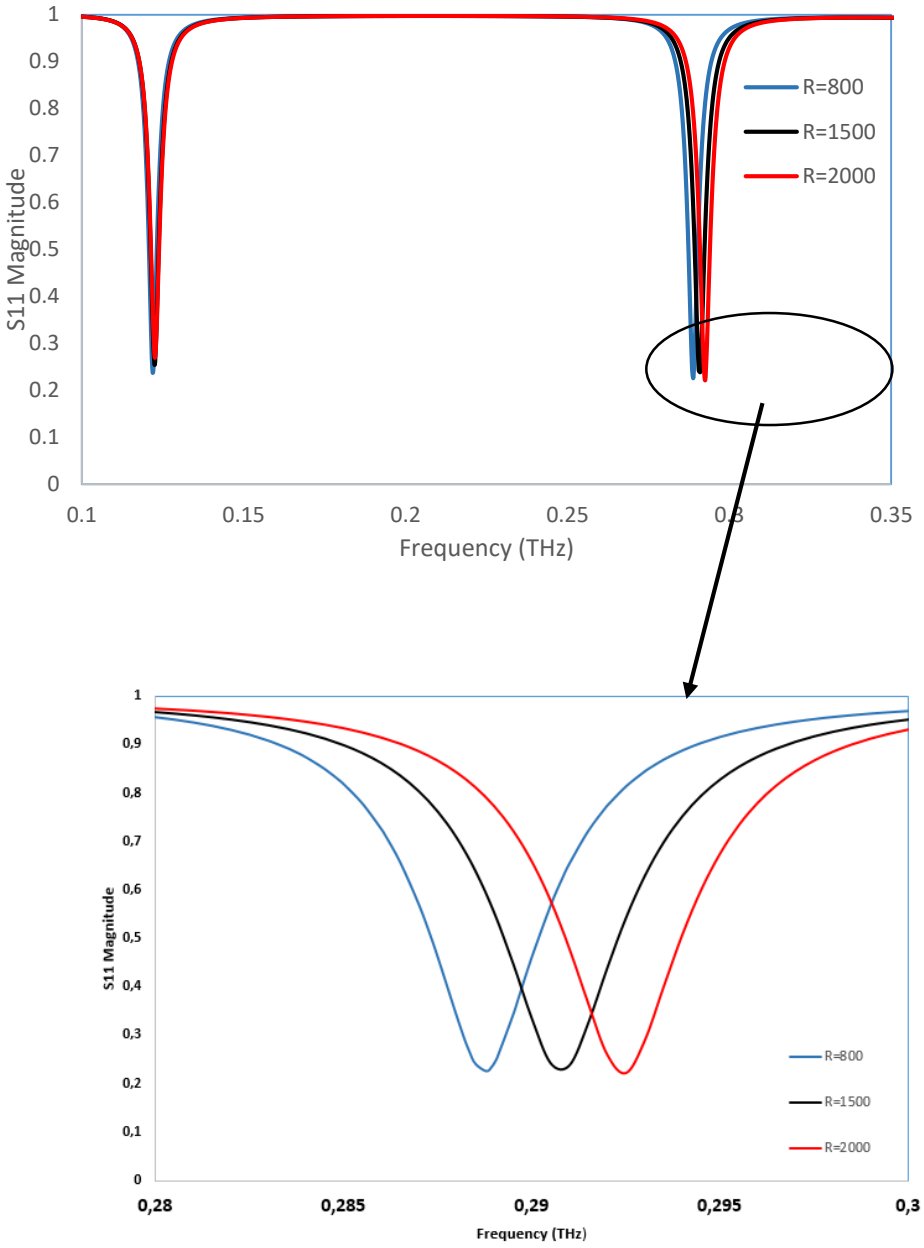

Figure 5-7 S11 parameters of complimentary H absorber with active diodes

As it can be seen from the Figure 5.7 the second resonance frequency is tuned in the right direction with the increase in the resistance. We can say that a 1kΩ increase in the resistance will shift the resonant 5 GHz. However, when the resistance of the diode is kept at a constant value and the capacitance is changed, no shift is occurred. This can be

explained with the capacitive behavior of the gaps. The gaps are acting as capacitors over the resonator and the effect of additional capacitors are negligible with compared to the effects of gaps.

5.4 Conclusion

In this chapter complimentary H-shape resonator within split square ring absorber is used for testing the tunability. Mechanical and Electrical tunability methods are implemented to the absorber structure, and the results indicate that purposed structure can operate at different frequencies by using variable tuning techniques. After the gathered results, the most useful method appeared as using MEMS and changing the gaps of the split square ring. Also, with changing the orientation of the design, two different resonances can be gathered; however, the loss in the magnitude is higher than the first method. On the other hand, the application with embedded diodes shows different results, declines in the magnitude is almost zero, but the shift is slightly lower than the other two methods. The proposed applications are promising for the structure to be used in different devices like antennas, active filters, tunable perfect absorbers and electro-optical switches.

CHAPTER 6: METASWITCH

Embedding materials that are sensitive to applied optical stimulus is a method for giving switch properties to MTMs. Inserting such photoconductive semiconductors to different parts of the MTMs gives the ability to control the response of the metamaterial structure. The material can be added as a substrate or as a layer between the substrate and the resonator [76, 77, 78]. In that application, it is easy to implement semiconductor to the structure, on the other hand, it is hard to control desired resonance because when the pump light applied to the structure, the whole response of the metamaterial will change. In order to solve this problem, the semiconductor can be inserted to the gaps of the resonator, which is a more complicated method in terms of manufacturing but in that case, we can make single switch operations. For a MTM structure that has two resonances, with an applied pump light we can dispute one of the resonance while the other kept at a constant frequency and magnitude [19, 79, 80]. For metallic split ring (SRR) metamaterials, gaps within the resonator act as capacitors that affecting the surface current distribution and also resonance response. So filling the gap with photoconductive semiconductors gives the ability to switch off the resonance response.

6.1 Silicon as Photoconductive Semiconductor

In this part, silicon is used as a photoconductive semiconductor to perform single and double switchable metamaterial properties. , and it is proved that single and double resonance switching is applicable with this technique [81, 82]. Electromagnetic response of proposed Fishnet and H-absorber structure are analyzed by integrating photoconductive

silicon as a layer between the polyimide substrate and gold resonator and also filling the gaps of the square ring resonator. The silicon that is used was chosen from the material library with pump-power dependent conductivity σsi and constant dielectric permittivity $\varepsilon_{si} = 11.7$.

6.2 Complimentary H Absorber Switch

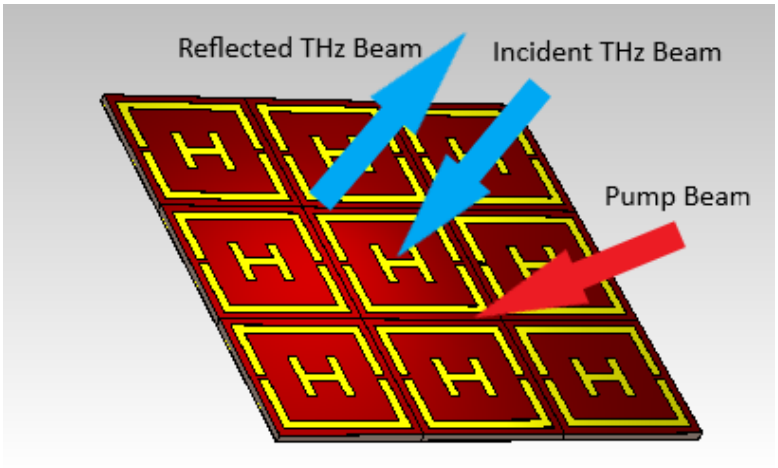

Figure 6-1 The view of planar array of silicon integrated absorber.

The first application has done for complimentary H-absorber structure by embedding silicon layer between polyimide substrate and resonator, which can be classified as double switching application. In Figure 6.1, the planar perspective of H-absorber structure is shared. With applying a pump beam to the planar structure, the σ_{si} of the silicon can be varied. The thickness of the silicon layer is set to 300 nm, which is the same thickness as the resonators.

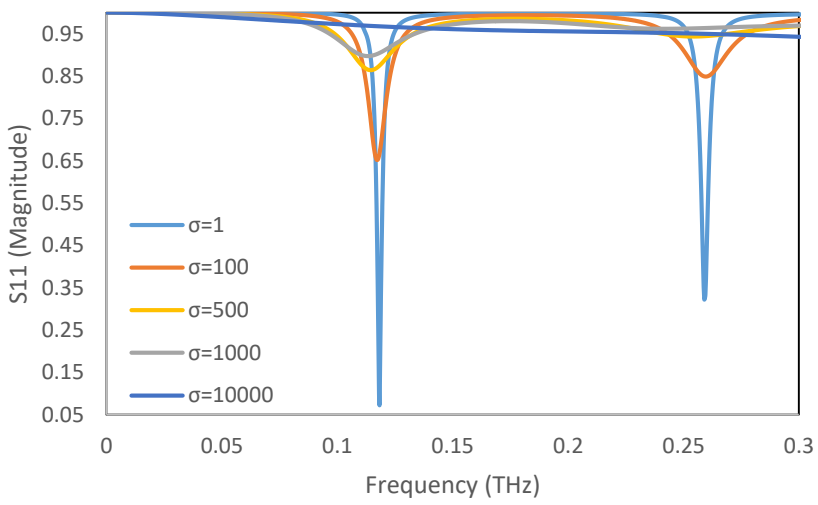

Figure 6-2 S11 parameters of silicon embeded complimentary H-absorber.

The current laser techniques give the ability to apply desired power through the pump beam to the silicon layer, which will adjust the conductivity of the silicon layer. For analysis, we changed the conductivity of silicon layer from the simulation program and checked the reflection response from S 11 magnitudes of the proposed structure. As it is presented in Figure 6.2 with the increase in the conductivity (σsi), which varies through the pump-beam, the complete response of resonator is changing. Two strong resonances are weakening with high conductivity values; that feature allows us to use the structure for double switch applications. At σ_{si} value of 10000 S/m, it can be seen from the figure that the S 11 becomes a straight line at a high magnitude which indicates that the reflection is high and the resonances are disappeared. However, for σsi values 1 to 1000 S/m the resonances are appearing, and with selecting required pump-beam, we can adjust our structure to absorb or reflect the incident THz light like a switch. However, the disadvantage of this application is the dependency of the resonances, if we desire to switch

off one resonance of the spectrum it is not possible because of the silicon layer that covers the whole structure under the resonator.

6.3 H Fishnet Switch

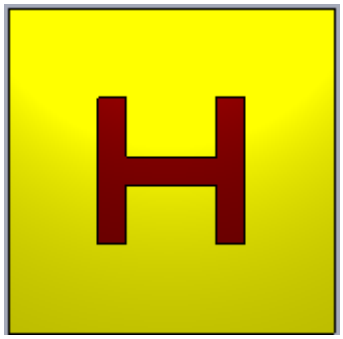

Figure 6-3 Front view of silicon embeded fishnet metamaterial.

Complimentary H-shaped fishnet metamaterial is also analyzed for switching application. The H shape gaps at the front and back side of the structure are filled with photoconductive silicon, and the conductivity of them changed through the applied electromagnetic beam. However, the area at the surface of the fishnet structure has less gap with compared to the absorber structure, and the absorption is still enough to be manipulated by an applied pump beam. The illustration of silicon embedded complimentary H fishnet structure is shared in Figure 6.3. The silicon surface increases the reflection of the design, but at the same time, it gives the ability to adjust the absorption rate. The reflection characteristics of the structure can be analyzed by using S11 parameters. It was an expected result to see a decrease in the absorption and increase in the reflection with compared to non-integrated silicon structure. In Figure 6.4, the S11 magnitudes via different silicon conductivity values are shared. From the figure, it can be seen that for 1 S/m silicon conductivity, the S11 magnitude is 0.85, which is way below than the previous results.

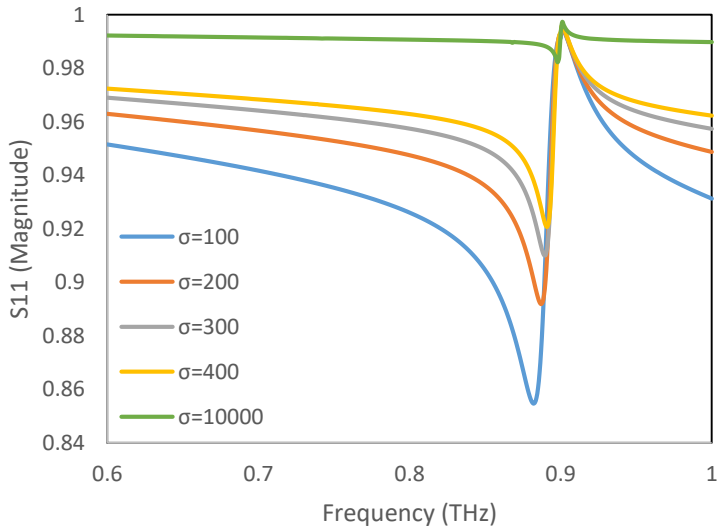

Figure 6-4 S11 magnitudes of silicom embeded fishnet metamaterial

The results are well matched with the theory and the reflection increased, which indicates the decrease in the absorption, with the change in conductivity of the silicon layer. It was essential to keep the resonance frequency stable, and if we check the Figure, the shift in the resonance frequency is negligible (around 1 GHz) for 1000 S/m difference in conductivity. The impedance match of the surface is disappearing as the conductivity of the surface increases with the applied pump beam, and this proves the capability of the design for switch application.

6.4 Conclusion

In this chapter, two optically controlled broadband metamaterial switches are demonstrated. The analysis indicates that the change in the electrical properties of the silicon layers can reduce the absorption rates without changing the resonance frequency, which provides switching dynamics to the proposed structures.

CHAPTER 7: CONCLUSION

7.1 The Conclusion of the Thesis

Promises of THz region increases the attention on that region and researchers are trying to develop highly efficient devices that operate with THz waves. Metamaterials provide innovative solutions for overcoming the problems that have been faced with THz radiation. However, the region lacks supplementary designs that will suit all applications in this region. The objective of the thesis was to introduce metamaterial structures that can cover the needs of the area, to achieve that goal, absorber sensor and switch applications for the proposed designs are presented in this thesis.

At the beginning of the thesis, the simulation software and the boundary conditions are introduced, and the designs are presented with the dimensions. After describing the analyzing approach, the metamaterial property (negative refractive index) of the structure is validated by using S-parameter retrieval method. At the strong resonant region, the results showed that both real parts of permittivity and permeability are negative.

The absorption characteristics of complimentary H Absorber and Complimentary H fishnet structures are analyzed in Chapter 3. Also, the physical characteristics of the designs are presented in this chapter by using the electric field and surface current distributions. The perfect absorption is achieved by 99% for complimentary H shape absorber and 97.3% for fishnet absorber in the Sub-THz regime.

Afterwards, the sensory application is conducted for two designs; the material to be detected is modelled as an overlayer on top from the simulation software. With changing the thickness and permittivity of the overlayer, the changes in the resonant frequencies are

investigated. For fishnet structure, both sides of the metamaterial can be used as a sensor which results with an increase in the sensitivity. The results show that the proposed designs have significant sensor abilities.

In order to extend the operation range of the metamaterial absorbers, mechanical and electrical tunability applications are tested in chapter 5. Firstly, MEMS are applied to complimentary H absorber to increase the gap between the outer square ring of the resonator. Then, tunability is achieved by changing the orientation of the planar structure, and lastly, the active diodes are implemented to the gaps of the outer square ring, and the tunability has achieved.

Finally, optical switch properties are analyzed by embedding silicon layers to both structures. The results demonstrate that both designs can be used as optical switches in the Sub-THz region. Ultimately, it can be concluded that two unique MTM structures have been introduced to the literature to be used in future researches.

Two journal papers from this thesis were published in Optik Journal Elsevier.

7.2 Future works

In this thesis, numerical and theoretical analysis of two metamaterial structures were carried out. The absorber, sensor and switch applications were made by using simulation software. However, to prove the applicability of the designs, experimental efficiency analysis, as well as experimental characterization, should be done as the future work.

References

[1] Ghann , William; Uddin, Jammal, in *Terahertz (THz) Spectroscopy: A Cutting-EdgeTechnology*, 2017.

[2] Bradley Ferguson, Xi-Cheng Zhang, "Materials for terahertz science and technology," *Nature Materials,* vol. 1, p. 26–33, 2002.

[3] G. P. Williams, "Filling the THz gap—high power sources and applications," *Rep. Prog. Phys.,* vol. 69 , p. 301–326, 2006.

[4] M. Tonouchı, "Cutting-edge THz technology," *Nature Photonics,* vol. 1, 2007.

[5] F. e. a. Oliveira, "Neural network analysis of terahertz spectra of explosives and bio-agents," *Proc. SPIE,* vol. 5070, no. , p. 60–70 , 2003.

[6] D. F. Zimdars, "pigtailed terahertz time domain spectroscopy instrumentation for package inspection and security imaging," *Proc. SPIE ,* vol. 5070, p. 108–116, (2003.

[7] J. F. e. a. Federici, "THz imaging and sensing for security applications—explosives, weapons and drugs," *Semicond. Sci. Technol,* vol. 20, p. 266–280, 2005.

[8] Rosker, Mark J; Wallece, H Bruce, "Imaging Through the Atmosphere at Terahertz Frequencies," *IEEE MTT-S International Symposium,* 2007.

[9] V. G. Veselago, "The Electrodynamics of Substances with Simultaneously Negative Values of E and M," *P. N. Lebedev Physics Institute, Academy of Sciences U.S.S.R. Usp. Fiz.,* vol. 92, pp. 517-526, 1964.

[10] Smith, D. R., Padilla, W. J., Vier, D. C, Nemat-Nasser, S. C, and Schultz, S., "Composite medium with simultaneously negative permeability and permittivity," *Physical Review Letters,* vol. 84, no. 18, p. 4184–4187, 2000.

[11] Shelby, R. A., Smith, D. R., and Schultz, S., "Experimental verification of a negative index of refraction," *Science,,* vol. 292, no. 5514, p. 77–79, 2001.

[12] Shelby, R. A., Smith, D. R., Nemat-Nasser, S. C., and Schultz, S., "Microwave transmission through a two-dimensional, isotropic, left-handed metamaterial," *Applied Physics Lett.,* vol. 78, no. 4, p. 489–491, 2001.

[13] Smith D. R., and Kroll, N., "Negative refractive index in left-handed materials," *Physical Review Letters,* vol. 85, no. 14, p. 2933–2936, 2000.

[14] F. Capolino, Aplications of Metamaterials, Metamaterials Handbook.

[15] Tao Chen, Suyan Li and Hui Sun, "Metamaterials Application in Sensing," *Sensors,* vol. 12, pp. 2742-2765, 2012.

[16] A. Ishimaru, S. Jaruwatanadilok and Y. Kuga, "Generalized surface plasmon resonance sensors using metamaterials and negative index materials," *Prog. Electromagn. Res.,* vol. 51, p. 139–152, 2005.

[17] Huda A. Majid, Mohamad Kamal A. Rahim, Thelaha Masri, "Left Handed Metamaterial Design for Microstrip Antenna Application," *RF and Microwave Conference IEEE International,* 2008.

[18] C. M. e. a. Watts, "Terahertz Compressive Imaging With Metamaterial Spatial Light Modulators," *Nature Photonics,* vol. 8, p. 605–609, 2014.

[19] H.-T. e. a. Chen, "Experimental Demonstration Of Frequency-Agile Terahertz Metamaterials," *Nature Photonics,* vol. 2, p. 295–298, 2008.

[20] Hu Tao, Nathan I. Landy, Christopher M. Bingham, Xin Zhang, Richard D. Averitt, and Willie J. Padilla; , "A metamaterial absorber for the terahertz regime: Design, fabrication and characterization," *Optics Express,* vol. 16, no. 10, pp. 7181-7188, 2008.

[21] N. I. Landy, S. Sajuyigbe, J. J. Mock, D. R. Smith, and W. J. Padilla;, " Perfect Metamaterial Absorber.," *Phys. Rev. Lett. ,* vol. 100, no. 207402 , 2008.

[22] X.-J. He, Y. Wang, J.-M. Wang, and T.-L. Gui, "DUAL-BAND TERAHERTZ METAMATERIAL ABSORBER WITH POLARIZATION INSENSITIVITY," *Progress In Electromagnetics Research,,* vol. 115, p. 381–397, 2011.

[23] Shuo Liu, Haibing Chen, Tie Jun Cui, "A broadband terahertz absorber using multi-layer stacked bars," *APPLIED PHYSICS LETTERS,* vol. 106, 2015.

[24] Tao Chen ,Suyan Li and Hui Sun, "Metamaterials Application in Sensing," *Sensors,* vol. 12, no. 3 , pp. 2742-2765, 2012.

[25] Nathaniel K. Grady, Jane E. Heyes, Dibakar Roy Chowdhury, Yong Zeng, Matthew T. Reiten, Abul K. Azad, "Terahertz Metamaterials for Linear Polarization Conversion and Anomalous Refraction," *Science,* vol. 340, no. 6138, pp. 1304-1307, 2013.

[26] Hu Tao , N. I. Landy , Kebin Fan , A. C. Strikwerda , W. J. Padilla, R. D. Averitt , Xin Zhang, "Flexible Terahertz Metamaterials: Towards a Terahertz Metamaterial Invisible Cloak," in *IEDM 2008 . IEEE International*, 2008.

[27] S. G. W. H. M. N. a. Y. L. Lei Wang, "Graphene-Assisted High-Efficiency Liquid Crystal Tunable Terahertz Metamaterial Absorber," *Optics Express,* vol. 25, no. 20, 2017.

[28] YuanYao, Shaopeng Li, Lei Zhu, Fengmin Wu, Xunjun He and Jiuxing Jiang , "Multi-Band Terahertz Metamaterial Absorber for Sensing Application," *Integrated Ferroelectrics ,* vol. 190, pp. 149-155, 2018.

[29] S. J. e. a. Park, "Detection Of Microorganisms Using Terahertz Metamaterials," *Sci Rep.,* vol. 4, no. 4988, 2014.

[30] S. J. Park, S. A. N. Yoon and Y. H. Ahn, "Dielectric constant measurements of thin films and liquids using terahertz metamaterials," *RSC Adv,* vol. 6, 2016.

[31] S. J. PARK,, "Sensing viruses using terahertz nano-gap metamaterials," *BIOMEDICAL OPTICS EXPRESS,* vol. 8, no. 8, 2017.

[32] T. &. C. S. Hand, "Characterization of tunable metamaterial elements using MEMS switches.," *IEEE Antennas Wireless Propag. Lett.,* vol. 6, p. 401–404 , 2007.

[33] H. Tao, "Reconfigurable terahertz metamaterials.," *Phys. Rev. Lett.,* vol. 103, 2009.

[34] W. M. e. a. Zhu, "Microelectromechanical Maltese-Cross Metamaterial with Tunable Terahertz Anisotropy," *Nat Commun.,* vol. 11, no. 3, p. 1274, 2012.

[35] Kivshar, Y. S. Zharov, A. A., Shadrivov, "Nonlinear properties of left-handed metamaterials.," *Phys. Rev. Lett,* vol. 91, 2003.

[36] Lapine, M., Gorkunov, M. & Ringhofer, K. H. , "Nonlinearity of a metamaterial arising from diode insertions into resonant conductive elements.," *Phys. Rev. E,* vol. 67, 2003.

[37] Shadrivov, I. V., Kozyrev, A. B., van der Weide, D. W. & Kivshar, Y. S. , "Tunable transmission and harmonic generation in nonlinear metamaterials," *Appl. Phys. Lett.,* vol. 93, 2008.

[38] V. A. Fedotov, "Temperature control of Fano resonances and transmission in superconducting metamaterials.," *Opt. Express ,* vol. 18, p. 9015–9019, 2010.

[39] B. B. Jin, "Low loss and magnetic field-tunable superconducting terahertz metamaterial.," *Opt. Express ,* vol. 18, p. 17504–17509 , 2010.

[40] S. H. Lee, "Switching terahertz waves with gate-controlled active graphene metamaterials," *NATURE MATERIALS ,* vol. 11 , 2012.

[41] Dibakar Roy Chowdhury, Ranjan Singh, Antoinette J. Taylor, Abul K. Azad, "Ultrafast Switching in Terahertz Metamaterials using Ion Implanted Silicon on Sapphire," *arXiv e-prints,* p. 1407.2715, 2014.

[42] Z. Rahimi., "The Finite Integration Technique (FIT) and the Application in Lithography Simulations.," 2011.

[43] Schuhmann R., Weiland T., "Recent Advances in Finite Integration Technique for High Frequency Applications.," vol. 4, 2004.

[44] D. Sievenpiper, L. Zhang, R. F. J. Broas, N. G. Alexopolous, and E. Yablonovitch, "High-Impedance Electromagnetic Surfaces with a Forbidden Frequency Band," *IEEE Transactions on Microwave Theory and Techniques,* vol. 47, pp. 2059-2074, 1999).

[45] S. Walia, C. M. Shah, P. Gutruf, H. Nili, D. R. Chowdhury, W. Withayachumnankul, M. Bhaskaran, and S. Sriram., " Flexible Metasurfaces and Metamaterials: A Review of Materials and Fabrication Processes At Micro- and Nano-Scales.," *Applied Physics Reviews ,* vol. 2, no. 011303, pp. 1-14, 2015.

[46] M. Gil, J. Bonache, F. Martín. , "Metamaterial filters: A review.," *Metamaterials,* vol. 2, p. 186–197, 2008.

[47] S. Gu, J. P. Barrett, T. H. Hand, B.-I. Popa, and S. A. Cummer., "A broadband low-reflection metamaterial absorber," *Journal of Applied Physics.,* vol. 108, no. 064913, pp. 1-6, 2010.

[48] K. Wu, Yo. Huang, T. Wanghuang, W. Chen, and G. Wen. , "Numerical and theoretical analysis on the absorption properties of metasurface-based terahertz absorbers with different thicknesses.," *Applied Optics. ,* vol. 54, p. 299, 2015.

[49] Y. Ra'di, C. R. Simovski, and S. A. Tretyakov. , "Thin Perfect Absorbers for Electromagnetic Waves: Theory, Design, and Realizations.," *Physical Review Applied.,* vol. 3, no. 037001., 2015.

[50] Jacob B. Khurgin, Greg Sun, "Scaling of losses with size and wavelength in nanoplasmonics and metamaterials," *Appl. Phys. Lett. ,* Vols. 99,, no. 211106, 2011.

[51] J. Valentine, S. Zhang, T. Zentgraf, E. Ulin-Avila, D. A. Genov1, G. Bartal, and X. Zhang,, "Three-Dimensional Optical Metamaterial With A Negative Refractive Index," *Nature,* vol. 455, p. 376–379, 2008.

[52] A. Mary, S. G. Rodrigo, F. J. Garcia-Vidal, and L. Martin-Moreno, "Theory of negative-refractive-index response of double-fishnet structures," *Phys. Rev. Lett.,* vol. 101, 2008.

[53] R. Marques, L. Jelinek, F. Mesa, and F. Medina, "Analytical theory of wave propagation through stacked Fishnet metamaterials," *Opt. Express,* vol. 17, p. 11582–11593, 2009.

[54] M. Kafesaki, I. Tsiapa, N. Katsarakis, T. Koschny, C. M. Soukoulis, and E. N. Economou, "Left-Handed Metamaterials: The Fishnet Structure and Its Variations," *Phys. Rev. B,* vol. 75, no. 23, pp. 235114,, 2007.

[55] Z. Jakšić, D. Tanasković, and J. Matović,, "Fishnet-Based Metamaterials: Spectral Tuning Through Absorption Mechanism," *Acta Phys. Pol. A,* vol. 116, no. 4, pp. 333-335, 2009..

[56] H. F. Álvarez, M. E. de C. Gómez and F. Las-Heras, "A Six-Fold Symmetric Metamaterial Absorber," *Materials,* vol. 8, pp. 1590-1603, 2015.

[57] J. Zhong, Y. Huang, G. Wen, "Single-/dual-band metamaterial absorber based on cross-circular-loop resonator with shorted stubs," *Applied Physics A,* vol. 108, p. 329, 2012.

[58] Hu Tao, C M Bingham, D Pilon, Kebin Fan, A C Strikwerda, D Shrekenhamer, WJPadilla, Xin Zhang and R D Averitt, " A dual band terahertz metamaterial absorber," *J. Phys. D: Appl. Phys. ,* vol. 43, no. 225102, p. 5, 2010.

[59] L.-L. W. G.-Z. W. W.-Q. H. X. Z. X.-F. L. Ben-Xin Wang, "Tunable bandwidth of the terahertz metamaterial absorber," *Optics Communications,* vol. 325, pp. 78-83, 2014.

[60] Na Liu, Stefan Kaiser, Harald Giessen, "Magnetoinductive and Electroinductive Coupling in Plasmonic Metamaterial Molecules," *Adv. Mater.,* vol. 20, p. 4521–4525, 2008,.

[61] J. Wang , "Tunable broad-band perfect absorber by exciting of multiple plasmon resonances at optical frequency," *Optics Express ,* vol. 20, no. 14, 2012.

[62] Y. Z. Cheng, "Ultrathin Six-Band Polarization-Insensitive Terahertz Perfect Metamaterial Absorber Based on a Cross-Cave Patch Resonator," *Materials,* 2017.

[63] . Z. Liao, "High-Order Localized Spoof Surface Plasmon Resonances and Experimental Verification," *Scientific Reports,* vol. 5, no. 9590, 2015.

[64] Najlaa Shawky, Salah Al-deen Adnan Taha, Hakan Altan, C. Sabah, "Single- and Double-Sided Sensor Applications of Metamaterials Based on Square-Ring And Diamond Resonators For Terahertz Region," *Modern Physics Letters B ,* vol. 31, no. 8, p. 14, 2017.

[65] O. Akgol, M. Karaaslan, E. Unal, C. Sabah, "Implementation of a perfect metamaterial absorber into multi-functional sensor applications," *Modern Physics Letters B,* vol. 31, no. 15 , 2017.

[66] C. Sabah, F. Dincer, M. Karaaslan, E. Unal, O. Akgol, E.Demirel, "Perfect metamaterial absorber with polarization andincident angle independencies based on ring and cross-wire resonators for shielding and a sensor application," *Opt. Commun. ,* vol. 322, p. 137–142, 2014.

[67] ,. V. ,. N. Cumali Sabah " ", "Realization of polarization-angle-independent fishnet-based waveguide metamaterial comprised of octagon shaped resonators with sensor and absorber applications," *Journal of Materials Science: Materials in Electronics,* vol. 27, no. 5, p. 47, 2016.

[68] C. Sabah, H.G. Roskos, "Terahertz Sensing application by using planar split-ring resonator structures," *Microsyst Technol,* vol. 18, pp. 1271-2076, 2012.

[69] Jeremiah P Turpin et al., "Reconfigurable and Tunable Metamaterials: A Review of the Theory and Applications," *International Journal of Antennas and Propagation,* 2014.

[70] N. Chikhi, Di Gennaro, E. Esposito, A. Andreone, "A study of Tunable Metamaterial Devices for THz Region," *Terahertz and Mid Infrared Radiation: Generation Detection and Applications,* 2011.

[71] Dongxing Wang, Lixin Ran, Hongsheng Chen, Mingkai Mu, Jin Au Kong, and Bae-Ian W, "Active left-handed material collaborated with microwave varactors," *Appl. Phys. Lett.,* vol. 91, no. 164101, 2007.

[72] Filippo Costa, Giuseppe Pietro Vastante, "Tunable High-Impedance Surface With a Reduced Number of Varactors," *IEEE Antennas and Wıreless Propagatıon Letters,* vol. 10, 2011.

[73] Tennant, A. and Chambers, B. , "A single-layer tuneable microwave absorber using an active FSS," *IEEE Microwave and Wireless Components Letters,* vol. 14 , no. 1, pp. 46-47.

[74] Limei Qi, Chao Li, Guangyou Fang, "Tunable Terahertz Metamaterial Absorbers Using Active Diodes," *International Journal of Electromagnetics and Applications,* vol. 4, no. 3, pp. 57-60, 2014.

[75] Filippo Costa, Simone Genovesi, Agostino Monorchio, Giuliano Manara, "A Circuit-Based Model for the Interpretation of Perfect Metamaterial Absorbers," *IEEE Transactions on Antennas and Propagation,* vol. 61, no. 3, 2013.

[76] Shen N-H, "Broadband blueshift tunable metamaterials and dual-band switches," *Phys. Rev. B,* vol. 79, no. 161102, 2009.

[77] Padilla W J, "Dynamical electric and magnetic metamaterial response at terahertz frequencies," *Phys. Rev. Lett.,* vol. 96 , no. 107401, 2006.

[78] Manceau J-M, Shen N-H,, "Dynamic response of metamaterials in the terahertz regime: blueshift tunability and broadband phase modulation," *Appl. Phys. Lett.,* vol. 96, no. 021111, 2010.

[79] Shen N-H, Massaouti M, "Optically implemented broadband blueshift switch in the terahertz regime," *Phys. Rev. Lett.,* vol. 106, no. 037403, 2011.

[80] Dimitrios C. Zografopoulos & Romeo Beccherelli, "Tunable terahertz fishnet metamaterials based on thin nematic liquid crystal layers for fast switching," *Scientific Reports,* vol. 5, no. 13137, 2015.

[81] Zongcheng Xu, Runmei Gao, "Photoexited Switchable Metamaterial Absorber at Terahertz Frequencies," *Optics Communications,* vol. 344, p. 125–128, 2015.

[82] Yu Wang, Jinwei Zhu, Hao Zhang,, "Optically controlled redshift switching effects in hybrid fishscale metamaterials," *AIP Advances,* vol. 8, no. 055319, (2018.